# FIRE DISTURBANCE MAPPING IN A NORTHERN BOREAL FOREST USING AVHRR/NDVI IMAGERY: COMPARING TECHNIQUES OF CHANGE DETECTION AND SUBSTRATE CORRECTION

Tarmo K. Remmel ©

A Graduate Thesis Submitted

In Partial Fulfillment of the Requirements

for the Degree of Master of Science in Forestry

Faculty of Forestry and the Forest Environment

Lakehead University

May 2000

# ABSTRACT

Remmel, T.K. 2000. Fire disturbance mapping in a northern boreal forest using AVHRR/NDVI imagery: comparing techniques of change detection and substrate correction. 98 pp. Advisor: Dr. A.H. Perera

Key words: boreal forest, fire, remote sensing, spatial coincidence.

Ontario's landmass north of 51° latitude has been designated as the least intensively managed zone with respect to fire protection. Consequently, large natural fires dominate the boreal landscape. This northern zone, comprising nearly 43-million hectares of primarily unmanaged boreal forest, is virtually inaccessible by road. Understanding the fire dynamics of such an extensive, unmanaged, and inaccessible forest is valuable for further ecological research.

Three methods of analyzing Advanced Very High Resolution Radiometer (AVHRR)/ Normalized Difference Vegetation Index (NDVI) imagery were compared for post-fire detection and mapping in northern Ontario. Exposed ground conditions, resulting from the removal of forest cover, can inflate derived AVHRR/NDVI values. Corrections for these effects were applied to test whether fire-mapping accuracy could be increased. The suitability of three threshold-driven change detection methods developed in Alaskan boreal forests were tested under northern Ontario conditions along with three corrections for substrate reflectance for 1992, 1993, and 1995 fire seasons. A factorial ANOVA statistical design was implemented to test equality among various spatial coincidence variables. Accuracy was assessed using a spatial database.

Existing fire detection and mapping methods using AVHRR/NDVI are not directly suitable for use in northern Ontario. Results indicate the superiority of a strict, single-threshold method for reducing false detection and the lenient double-threshold method for increasing mapped area for each fire. Furthermore, strong correlation was found between fire size and the area detected to represent them; however, corrections for substrate reflectance did not significantly increase detection and mapping accuracy.

TABLE OF CONTENTS

TABLES

FIGURES

ACKNOWLEDGEMENTS

I am delighted to take this opportunity to thank the many people who provided support, guidance, and encouragement towards this project. My sincerest gratitude is expressed to my advisor, Dr. Ajith Perera, whose enthusiasm toward science, ability to motivate, and provision of many wonderful learning experiences enabled a productive and stimulating research environment. I also thank the Ontario Ministry of Natural Resources for the research grant that provided financial assistance throughout the course of this research project.

I extend many thanks to my committee members: Dr. Ulf Runesson (Associate Professor, Faculty of Forestry and the Forest Environment, Lakehead University) and Dr. David Euler (Dean, Faculty of Forestry and the Forest Environment). Their enthusiasm, constructive criticism, and valuable input helped me greatly throughout the research process. Thanks also to Dr. Phil Howarth (Geography Chair, University of Waterloo) for his valuable comments as the external examiner.

I would also like to thank Dave Schroeder, Kevin Weaver, Dennis Yemshanoff, Frank Schnekenburger, David Baldwin, Zbigniew Brodzik, and Abby Obenchain, at the Ontario Forest Research Institute, along with Jim Baker of the Ministry of Natural Resources' Forest Management Branch, for their countless reviews, advice, assistance, and encouragement. Finally, I thank my family and friends, who always supported and believed in my abilities.

# CHAPTER 1 – INTRODUCTION

## BACKGROUND

To prioritize protection from wildfire in Ontario's forests, fire managers have designated three fire management zones (described in Martell and Boychuk 1997) as shown in Figure 1. The dominantly southern zone is one of *intensive* fire control, aimed at protecting the high human population and associated values. The *measured* zone, primarily a region of sustainable forest licenses (SFLs), has experienced continued increases in control to protect valuable forest resources. The northernmost or *extensive* zone is subjected to low fire control because of sparse settlements and values and inaccessibility by road. Thus, most fires occurring within the nearly 43-million hectare unmanaged boreal forest are left to burn without any control and with modest monitoring.

Given the minimal level of monitoring in the extensive zone, little is known about the occurrence and spatial distribution of fires during or shortly after disturbance events. The potential expansion of native forestry operations into this zone emphasizes the need to know where resources exist and what quantities have been destroyed by fire (E.A. 107, Environmental Assessment Board 1994). With nearly three-million hectares burned in the extensive zone during the past half century alone (Perera *et al.* 1998), methods for providing accurate and efficient means of fire disturbance mapping are becoming increasingly essential.

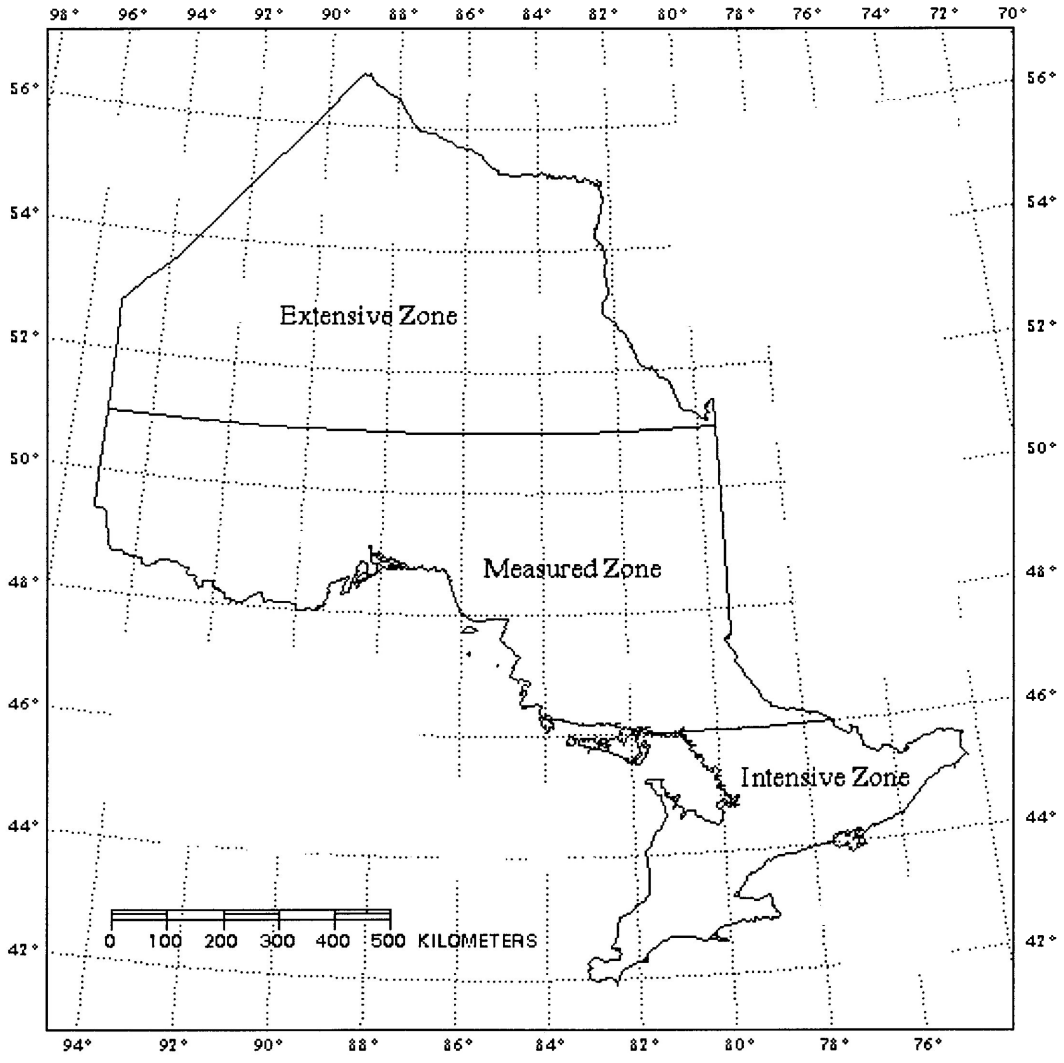


Figure 1. Generalized fire protection zones in Ontario, Canada (after Perera *et al.* 1998).

Fires are a tremendous force of change in the boreal ecosystems of northern Ontario. Given their magnitude, they can result in significant changes to landscape patterns, habitats, hydrological regimes, and natural resources availability (DeBano *et al.* 1998). Until recently, forest research has focused on the managed boreal forest, approximated by the measured zone of fire protection (Figure 1). However, the unmanaged, inaccessible, and extensive northern boreal forest provides an excellent opportunity to gain new ecological knowledge about natural fire regimes.

In Ontario, "the long term health and vigor of Crown forests should be provided for by using practices that, within the limits of silvicultural requirements, emulate natural disturbances and landscape patterns while minimizing adverse effects on plant life, animal life, water, soil, air and social and economic values, including recreational values and heritage values" (Crown Forest Sustainability Act, Statutes of Ontario 1994, Chap. 25). Therefore, knowledge of the northern fire regime would assist with forest management planning within the legal framework for Ontario.

Information about forest biomass burning has allowed estimates of gaseous emissions (Cahoon *et al.* 1994) and carbon fluxes (French *et al.* 1996; Burke *et al.* 1997; Zepp *et al.* 1997). The release of carbon and subsequent sequestering after re-vegetation are important parameters for ecological modelling of boreal ecosystems. The ability to calculate carbon and aerosol fluxes provides avenues for studying atmospheric composition, climate change, and forest productivity.

The random and vast spatial distribution of fires requires efficient mapping techniques that work for the entire extensive zone. Moreover, the harsh geography of northern landscapes hinders field mapping, making remotely sensed imagery the best choice for meeting these goals (Iverson *et al.* 1989). The low probability of obtaining cloud-free imagery and difficulties with mapping entire active fires further demonstrate the necessity of detecting post-fire disturbance patches, especially when fires extinguish before useable imagery is obtained. Thus, the current study compared methods to overcome obstacles of extent, timing, and removal of cloud cover with coarse spatial resolution, single-scene composite imagery (Holben 1986).

The *Advanced Very High Resolution Radiometer (AVHRR)* facilitates observation of spatially extensive areas (Roller and Colwell 1986; Teuber 1990) at approximately 1.1 $km^2$ resolution on a twice-daily basis. Thus, AVHRR images reduce data volume, analysis time, number of required images, and, therefore, the costs involved with obtaining, edge matching, and interpreting data. AVHRR imagery is easily accessible and costs approximately $\$0.0001/km^2$ (Lunetta and Elvidge 1998). Furthermore, the *Normalized Difference Vegetation Index (NDVI)* can be calculated from AVHRR's red (R) and near-infrared (NIR) channels for tracking reductions in vegetation, a common effect of fire.

Inflated NDVI values can result where ground conditions greatly influence the R and NIR reflectance components. For example, if the forest canopy is not closed, non-green reflectances from terrestrial soils and bedrock may reach the AVHRR sensor. Since soil and vegetation that is green have similar reflectance patterns in the stated spectral

regions (low in R, higher in NIR), soil/vegetation confusion can result. Thus, the magnitudes and differences between the spectral components are evaluated for correcting background reflectance effects. Three corrections are presented in this study.

Significant NDVI declines have been associated with vegetation disturbance patterns (e.g., Nemani and Running 1997), which include wildfires. Thresholds to measure NDVI decline have been established for mapping large boreal wildfires in Alaska (Kasischke *et al.* 1993; Kasischke and French 1995). Such thresholds are used to decide whether vegetation greenness between two dates has decreased sufficiently to be considered a fire disturbance. In the current study, these methods were applied in northern Ontario to compare their accuracy for similar purposes.

Fires were ground-truthed using a comprehensive *geographic information system (GIS)* database of fire patterns, which contained dates and locations of fires in Ontario between 1921 and 1995 and was compiled from hardcopy maps derived from field data, aerial photographs, and interpretation of Landsat images (Perera *et al.* 1998).

This study compared the accuracy of fire mapping among three substrate corrections in conjunction with three AVHRR/NDVI threshold methods for the 1992, 1993, and 1995 fire seasons in northern Ontario.

## GOAL AND OBJECTIVES

The goal of this study was to compare the spatial coincidence among fires mapped with various substrate-corrected and uncorrected NDVI change-detection methods and the ground-truthing data. The methods were applied to mapping post-fire disturbance patches in northern Ontario for the 1992, 1993, and 1995 fire seasons. Three objectives were identified: to compare the accuracy of fire mapping from the (1) *sensor*, (2) *event*, and (3) *truth* perspectives. The objectives included comparisons from the general treatment level (*sensor*, *event*, and *truth* perspectives), followed by detailed fire-by-fire level comparisons (*event* and *truth* perspectives). Detailed comparisons of the sensor perspective were omitted due to data limitations (discussed under *Methods*).

### 1.2.1 Hypotheses

Given the goal and objectives for comparing the accuracy of fire mapping in northern Ontario, several null and alternate hypotheses were formulated for each accuracy measurement (described under *Methods*). Two null hypotheses were constructed, indicating equalities among (1) the effects of the three threshold methods and (2) the effects of the three substrate corrections. Alternate hypotheses implied that for either the threshold methods, or substrate corrections, at least one of the three effects differed from the others. For treatments rejecting a null hypothesis, further statistical tests were conducted to denote the specific treatment effects that differed.

## STUDY AREA

The study area encompassed lands north of the Area of the Undertaking (Environmental Assessment Board 1994) in the province of Ontario, Canada (Figure 2). The southern boundary of the study area is 51°N, approximating the northern limit of SFLs. The study area lacks road access and contains a few, small sparsely distributed communities.

In northern Ontario, topography is dominated by lakes and bedrock to the west and flat wetland plains to the east. Precipitation for the region varies between 450 and 800 mm annually. The cool mean-annual temperatures and extreme summer/winter fluctuations provide ideal growing conditions for boreal forest species (Ecological Stratification Working Group 1996). Boreal species are typified by black spruce (*Picea mariana* [Mill.] BSP), white spruce (*Picea glauca* [Moench] Voss), jack pine (*Pinus banksiana* Lamb.), balsam fir (*Abies balsamea* [L.] Mill.), tamarack (*Larix laricina* [Du Roi] K. Koch), white birch (*Betula papyrifera* Marsh.), and poplar species (e.g., *Populus tremuloides* Michx., *Populus balsamifera* L.) (Farrar 1995).

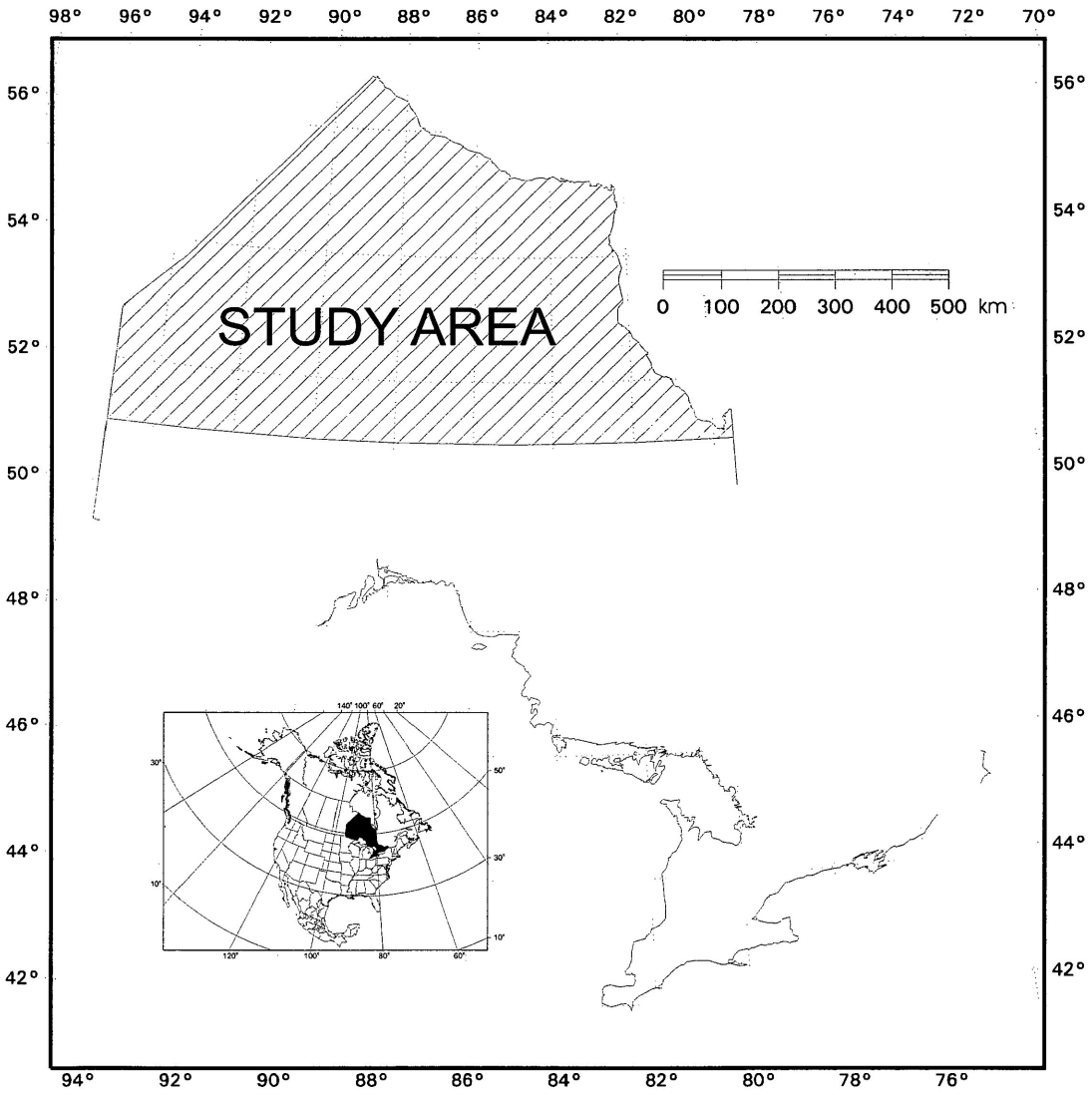


Figure 2. Study area location in Ontario, Canada.

Soils of northern Ontario are characterized by brunisols and podzols, with interspersed pockets of luvisols and organics (mesisols) (Agriculture and Agri-Food Canada 1996). Acidic brunisols and podzols occurring in mesic to arctic conditions regularly exhibit the strong brown chroma characteristic for the boreal region (resulting from high Fe and Al content). The eastern lowlands are dominated by undecomposed organic fibrisols, and the northern provincial limit is covered by extensive cryosols. Cryosols, common to northern boreal/barren landscapes, are underlain by permafrost and are subjected to cryoturbation. Pockets of luvisols characterized by thin layers of decomposing leaf litter also exist. Regosols and gleysols are rare within the study area.

The boreal forest pattern is changed by disturbances, fire being a major constituent (Whelan 1995). Seasonal electrical storms, declining northward, initiate fires accounting for over 90 percent of the area burned (Johnson 1992); the rest have anthropogenic origins (Heinselman 1981). The average fire frequency is 50–200 years (Heinselman 1981; Bergeron *et al.* 1999); however, in regions of intensive fire suppression, frequencies are closer to 500–1000 years (Lynham and Stocks 1991).

# CHAPTER 2 – DETECTING AND MAPPING FIRE DISTURBANCES

Fire detection and mapping can be conducted for either active fires or post-fire disturbance patches. Active fire observation is usually satellite-based and relies on thermal or optical techniques. Three primary categories of post-fire mapping methods exist: field, airborne, and satellite based.

## ACTIVE FIRE DETECTION

### 2.1.1 Thermal and Optical Methods

Thermal and middle infrared imagery have been used in many fire detection and mapping studies (e.g., Matson *et al.* 1987; Pereira and Setzer 1993a; Pozo *et al.* 1997), allowing drastic thermal gradients between fires and non-fires to be detected. Real-time detection of boreal forest fires using infrared and thermal data has been very successful (Justice *et al.* 1996; Rauste *et al.* 1997). Natural Resources Canada, in conjunction with the Canada Centre for Remote Sensing, is now developing *M3*, a project to display fire hotspots in real time (*http://fms.nofc.cfs.nrcan.gc.ca/FireM3/*) from AVHRR multispectral imagery on the Internet.

*Nighttime Defense Meteorological Satellite Program (DMSP)* optical images have been used to detect the high contrast between bright, active fires and the dark landscape (Ehrlich *et al.* 1997). This *instance in time* mapping depicts only areas currently burning, not necessarily the entire disturbance event during a specific satellite pass. Thus, the potential of this technique for mapping entire fire disturbances is low.

Although thermal imagery is better suited for fire detection than mapping, benefits are also noted for isolating cloud in images, indicating the need for compositing, and making atmospheric corrections (Flasse and Ceccato 1996). Robinson (1991) provides a thorough review of projects using infrared data for fire detection.

## 2.2 POST-FIRE DISTURBANCE DETECTION

### 2.2.1 Field and Airborne Methods for Mapping Fire Disturbances

Field surveys and airborne techniques are highly localized. In the past, post-fire mapping efforts involved field (Gillis and Leckie 1996) or aerial surveys, and disturbance patches were sketched by hand onto forest and highway maps (Williams 1953). Field surveys were conducted immediately after a fire disturbance or during its suppression to minimize effects of re-growth on mapping accuracy. The current forest resources mapping standard in Canada is based on aerial-photograph interpretation (Madill and Aldred 1977; Gillis and Leckie 1993).

Modern mapping methods involve the use of helicopters and field crews outfitted with global positioning system (GPS) units to trace disturbance perimeters (Gillis and Leckie 1996). Then, the collected digital data are imported for use in a GIS. Gillis and Leckie (1996) also proposed methods for using digital frame cameras or video to replace conventional photography and eliminate the need to scan photos (King 1995).

Dendrochronological fire histories have been constructed using cross-sections of surviving trees in Ontario (e.g., Guyette and Dey 1995), providing records of cyclic fire

activity. In Alberta, lake-bottom sediment cores were used to predict hundreds of years of site-specific fire history from pollen and charcoal inclusions (MacDonald *et al.* 1991; Larsen and MacDonald 1998). These methods provide general indications of fire calendar for large fire events, but are unusable for precise fire mapping. Landry *et al.* (1995) studied C-band HH-polarized radar images of Saskatchewan to develop methods of extracting fire disturbances and found that disturbances were easier to detect in the year following a fire event.

### 2.2.2 Satellite Methods for Mapping Fire Disturbances

The 1972 launch of the first Landsat series satellite led to a new era of data collection. Landscape-scale digital forest-data could be collected and used for type classification (Dodge and Bryant 1976; Beaubien 1979), change detection, and disturbance recognition (Iverson *et al.* 1989).

Many researchers have been working on projects to detect fire disturbances from space. Pereira and Setzer (1993b) determined that *Thematic Mapper (TM)* band 4 was very useful for fire scar detection in Amazonia. Adding terrain data to TM imagery of New Mexico allowed Medler and Yool (1997) to increase the accuracy of supervised fire detection by 40 percent (as observed in the accuracy measure Kappa); they reasoned that terrain confines and directs the pattern of wildfire. Jakubauskas *et al.* (1990) found that timing imagery to allow complete vegetation mortality after a disturbance greatly improves the accuracy of disturbance mapping but Martín and Chuvieco (1995) found that it must be conducted before vegetation begins to recover. Woodcock *et al.* (1994)

conducted separate classifications for "poorly" and "well" illuminated image regions to reduce shadow effects and thus misclassification errors. The application of a multisensor approach in Africa combined fine and coarse spatial resolution data, removing biases of data supplied from different sources (Eva and Lambin 1998). This multisensor method indicated that middle-infrared (1.1 to 3.0 μm) observations, not available on some common platforms, greatly enhance burned-area detection.

The FireSat satellite is now being developed for continuous monitoring of global fire regimes (Levine *et al.* 1996). Although the emphasis is on active fires, some of the research is directed at detecting fire scars using various combinations of optical and infrared channels. An Alaskan RADARSAT study is also striving to simplify fire disturbance detection by comparing incidence angles, observed backscatter, and the relative differences between burn scars and forested areas (French *et al.* 1999). The FireSat and RADARSAT methods are still in their early stages of development.

#### 2.2.2.1 Remote Sensing Change Detection

During the 1980s, change detection concentrated on the then-new MSS and TM imagery. Primary processing techniques involved *principal component (PC)* analysis, finding axes 3, 4 and 5 to provide useful information on vegetation change (Bryne *et al.* 1980), allowing Richards and Milne (1983) to map burned areas in Australia. Forest mortality mapping in the Lake Tahoe basin (Collins and Woodcock 1996) and in Arizona (Patterson and Yool 1998) have relied on various orthogonalization techniques (i.e., multi-temporal Kauth-Thomas transformation, PC analysis, and Gram-Schmidt

orthogonalization). Results showed that soil and vegetation moisture, both greatly affected by fire, could alter spectral signatures.

An effort to map burns and their severity in Michigan (Jakubauskas *et al.* 1990) used a ratio of Landsat's Multi-Spectral Scanner (MSS) bands 7/5. The resulting image was smoothed using a 3×3 majority filter and further classified using unsupervised methods to generate both pre- and post-fire raster images. A GIS was used to compare the paired images.

Patterson and Yool (1998) emphasized the need for high spatial, radiometric, and spectral resolution. Milne (1988) indicated that radiometric, temporal, spatial, and registration accuracy factors are important considerations for digital change-detection research. The most important factor is knowledge of the environment being examined, especially when several scales are introduced simultaneously or comparisons are made between projects.

#### 2.2.2.2 AVHRR's Role in Vegetation Studies

National Oceanic and Atmospheric Administration's (NOAA) meteorological satellites have been utilized for vegetation studies at global (Agbu and James 1994), regional (Loveland and Belward 1997), and provincial scales (examples follow). Of primary appeal is NOAA's AVHRR, operating in visible, infrared, and thermal regions of the electromagnetic spectrum.

Four daily passes of the NOAA satellites, coupled with spatial resolutions ranging from 1–8 km and a 9-million $km^2$ coverage, have provided numerous vegetation monitoring and data collection opportunities worldwide. Significant vegetation change studies using AVHRR have been conducted in Africa (Gatlin *et al.* 1983; Tucker *et al.* 1985; Townshend and Justice 1986; Eva and Lambin 1998), Spain (López *et al.* 1991; Gonzalez-Alonso *et al.* 1996; Fernandez *et al.* 1997), Alaska (Kasischke *et al.* 1993; Kasischke and French 1995; French *et al.* 1995; Kasischke and French 1997), and Canada (Steyaert *et al.* 1997).

The International Geosphere Biosphere Program has drafted several standards and goals for AVHRR 1-km remote sensing of the earth (Townshend *et al.* 1994), which are reflected in many of the aforementioned studies. Price (1987) provides detailed pre-launch calibration information for the AVHRR sensor: Vibrations during launching can compromise these calibrations, indicating the need for further calibration after satellite deployment (Eidenshink and Faundeen 1994).

### 2.2.3 Vegetation Indices for Quantifying Greenness

Fire destruction of vegetation usually begins with litter, foliage, and branches (Johnson 1992). Destruction of foliage containing chlorophyll changes the normally observed R/NIR reflectance ratio for green vegetation. Based on this premise, the use of a vegetation index that is sensitive to the R and NIR regions of the electromagnetic spectrum is suited to quantifying vegetation change (Horler *et al.* 1983).

Over the past three decades, many indices have been developed to summarize multispectral vegetation data (Appendix I). Most are either ratios or difference measures. Perry and Lautenschlager (1984) summarize many of these indices and indicate equivalencies among them. Due to its simplicity, NDVI is the most widely used.

#### 2.2.3.1 Normalized Difference Vegetation Index

The values required to calculate NDVI are reflectance values from the R and NIR portions of the electromagnetic spectrum for each pixel:

$$NDVI = (NIR-R)/(NIR+R) \quad (1)$$

The computed NDVI values range from -1.0 to +1.0 and describe the relative greenness of the represented area. The continuum of positive NDVI values represents a gradient of increasing greenness, often associated with the abundance of vegetation that is green (chlorophyll). Negative values commonly indicate clouds, haze, snow, ice, or rock. Calculation of the NDVI has been applied to MSS (e.g., Rouse *et al.* 1973), TM (e.g., Marsh *et al.* 1992), SPOT HRV (e.g., Larsson 1993), and AVHRR (e.g., Eastman and Fulk 1993) imagery. A comprehensive review of NDVI calculation, precision, and error is provided by Roderick *et al.* (1996).

To obtain meaningful NDVI values for vegetation monitoring, the NIR component for each pixel must be greater than the corresponding R component. This property is best

described with a diagram displaying the spectral reflectance of typical vegetation that is green, in the visible and NIR regions of the electromagnetic spectrum (Figure 3).

Vegetation that is green, reflects little in the R portion of the spectrum and highly in the NIR (Goward *et al.* 1985). This characteristic difference ($\Delta$) is measured and normalized by dividing by the sum of R and NIR reflectances. The resulting NDVI represents the ratio of reflectance change compared with total reflectance, reducing the bias of reflectance magnitude. The NDVI ratio reduces background noise; however, further stratification by species could greatly assist interpretation by minimizing differences in optical properties stemming from physiognomic variances (Leblanc *et al.* 1997).

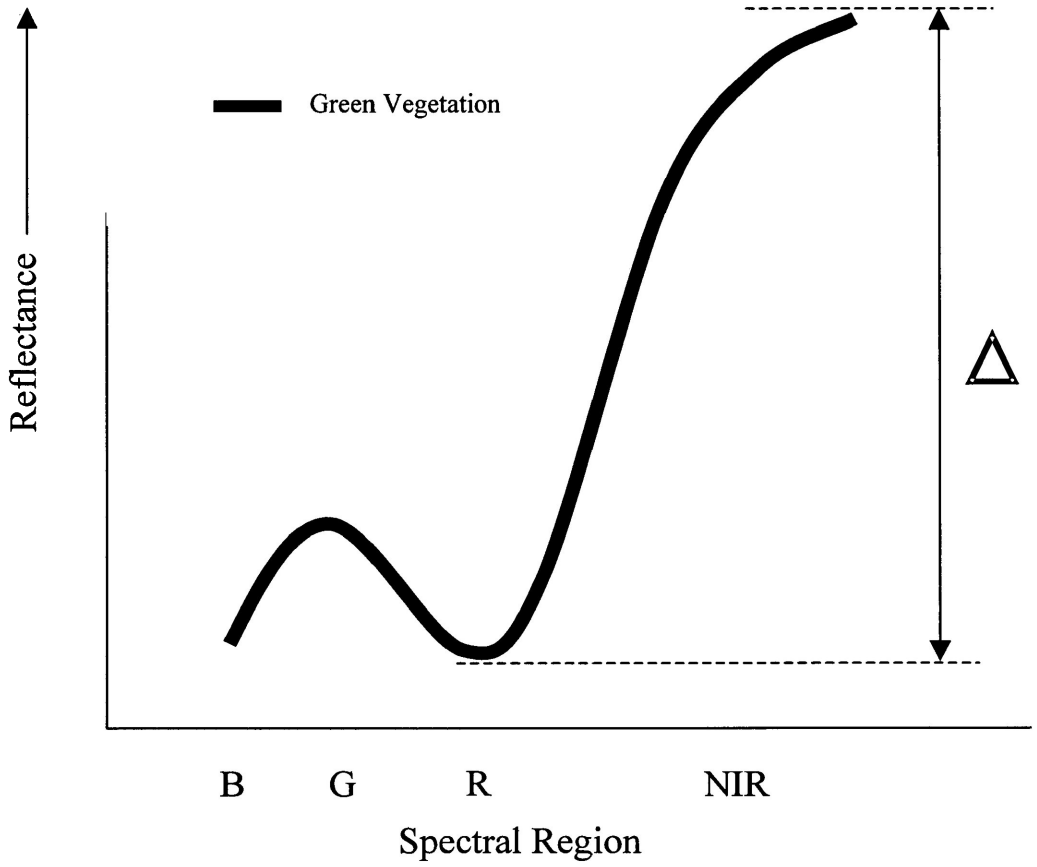


Figure 3. Reflectance curve of typical green vegetation in the visible and NIR regions of the electromagnetic spectrum (after Y. Li *et al.* 1993). (B), (G), (R), and (NIR) represent the blue, green, red, and near-infrared regions of the electromagnetic spectrum respectively; (Δ) is the difference in reflectance for typical green vegetation between the R and NIR spectral regions.

In Spain, NDVI imagery derived from the AVHRR sensor has proven successful for detecting fires from 14 000 to 26 000 ha, using image subtraction with thresholds indicating significant change (Fernandez *et al.* 1997). In tropical regions, NDVI images have shown drastic contrast between burned and unburned sites (Razafimpanilo *et al.* 1995). Severe burns appear more likely to be classified correctly, because the low quantity of remnant vegetation is less likely to confuse the vegetation index. NDVI generated from TM imagery allowed Viedma *et al.* (1997) to monitor vegetation recovery after fire disturbances in Spain. More recently, Pereira (1999) concluded that NDVI did not perform well in areas of little or no vegetative cover, especially where there was much exposed soil.

Boreal forest fire detection methods have also been developed, mainly in Alaska but also in central Canada. A 1990–1992 study with AVHRR in Alaska arrived at a detection accuracy > 83% for all fires > 20 000 ha (Kasischke and French 1995). Fire events were detected by image subtraction and through setting NDVI change thresholds; detection was possible because scars showed significantly reduced NDVI compared to unburned areas. Kasischke *et al.* (1993) were able to detect 89.5% of Alaskan fires > 2 000 ha in size by using similar methods and without experiencing false detection. Furthermore, the general shapes of detected fires were consistent with ground-truthing data collected by field observers. Further studies have aimed at reducing cloud and atmospheric effects or by combining sequential seasons' data to monitor delayed green-up on disturbed patches (French *et al.* 1995).

Canadian studies have concentrated primarily on the Boreal Ecosystem-Atmosphere Study (BOREAS) sites in central Saskatchewan and Manitoba (Z. Li *et al.* 1997; Steyaert *et al.* 1997). Temporal AVHRR/NDVI composites of the BOREAS sites were used to detect burned areas indicated by decreased NDVI values. Z. Li *et al.* (1997) examined the area under the temporal NDVI curves for the fire seasons before and after the study period to make robust decisions on areas flagged as disturbance sites. They also used middle infrared data to assist with detecting active fires on single-date images. Steyaert *et al.* (1997), although more concerned with land cover mapping, noted vegetation return and its relationship with NDVI when mapping burned areas.

#### 2.2.3.2 Soil Background Effects on Vegetation Indices

Soils and vegetation that is green have different spectral signatures (Figure 4); however, they are generally similar in the R and NIR spectral regions (low R, higher NIR). Typically, soils reflect much higher in the R region than vegetation that is green, but sensors that view only broad slices of the electromagnetic spectrum and cannot synthesize hyperspectral soil or vegetation curves needed for more rigorous interpretation may confuse the two, resulting in inflated NDVI values (Huete and Tucker 1991).

Soil exposure can influence NDVI values when NIR > R, such that their difference (NIR-R) and R exhibit low values. Thus, to put NDVI into the proper context, the absolute magnitude of R and difference between R and the NIR values should be considered.

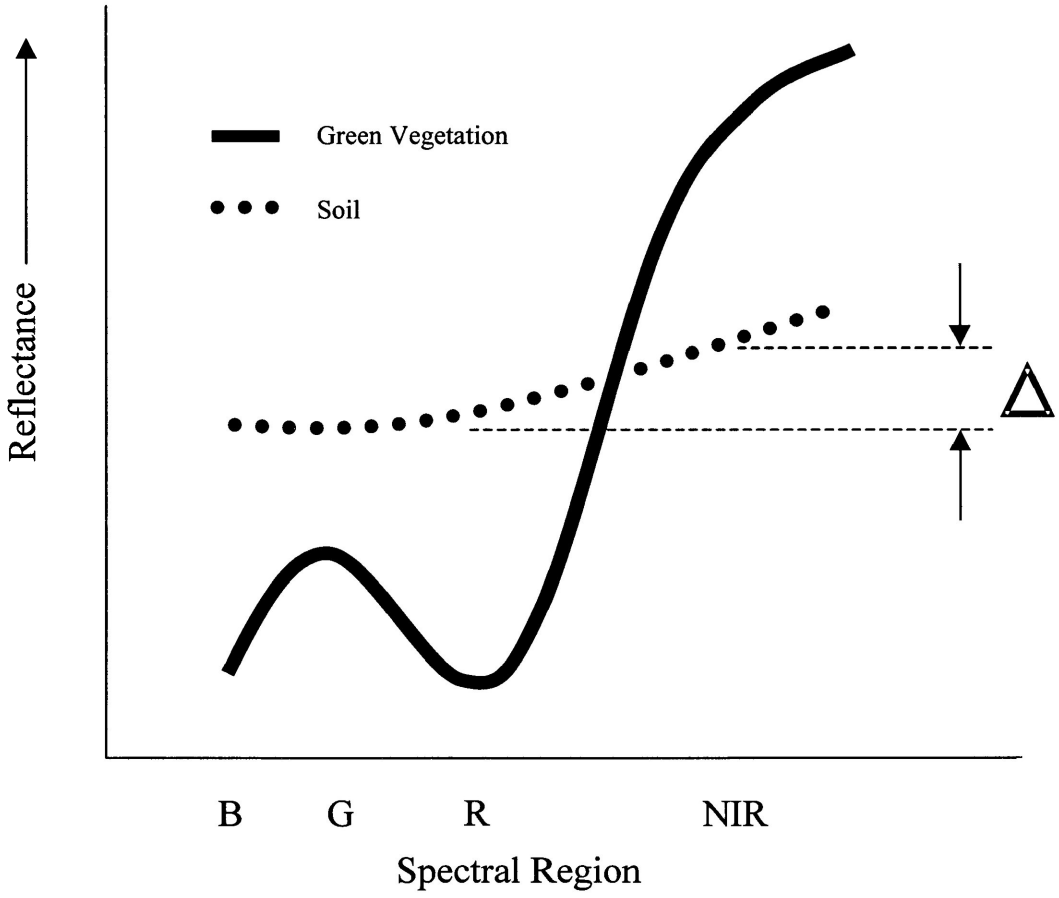


Figure 4. Reflectance curve of general soil types, with typical green-vegetation reflectance curve as reference in the visible and NIR regions of the electromagnetic spectrum (after Lillesand and Kiefer 1994). (B), (G), (R), and (NIR) represent the blue, green, red, and near-infrared regions of the electromagnetic spectrum respectively. (Δ) is the difference in reflectance for general soil types between the R and NIR spectral regions.

An early and successful attempt to understand soil effects in agricultural studies was made by Kauth and Thomas (1976) with the introduction of the *tasseled cap (TC)* transformation for TM and MSS platforms. This transformation generates several indices, of which soil brightness and green vegetation are most important. Extensive testing under agricultural conditions has proven this technique successful; nevertheless, the TC has not been applied to AVHRR imagery or forested landscapes.

Two prominent vegetation indices consider the effect of soil reflectance on the index value for vegetation greenness: the *perpendicular vegetation index (PVI)* (Richardson and Wiegand 1977) and the *soil adjusted vegetation index (SAVI)* (Huete 1988). Of the two, PVI is the most common, accounting for soil background effects by basing its discrimination on a datum known as the *soil line* (Figure 5), a hypothetical line along which the R and NIR reflectance values of general soil types align when plotted in two-dimensional space (Huete and Tucker 1991). Mechanics indicate that dryer soils plot higher in R and NIR, while wetter soils plot lower. Therefore, the soil line represents a continuum of soil moisture regimes. Vegetation is indicated by NIR and R pairs plotting above the soil line (low R and high NIR reflectance). A gradient is formed perpendicularly upward from the soil line indicating increasing vegetative cover. This allows distance from soil-line thresholds to be selected for classifying percentage cover, which can be influenced by fire disturbances.

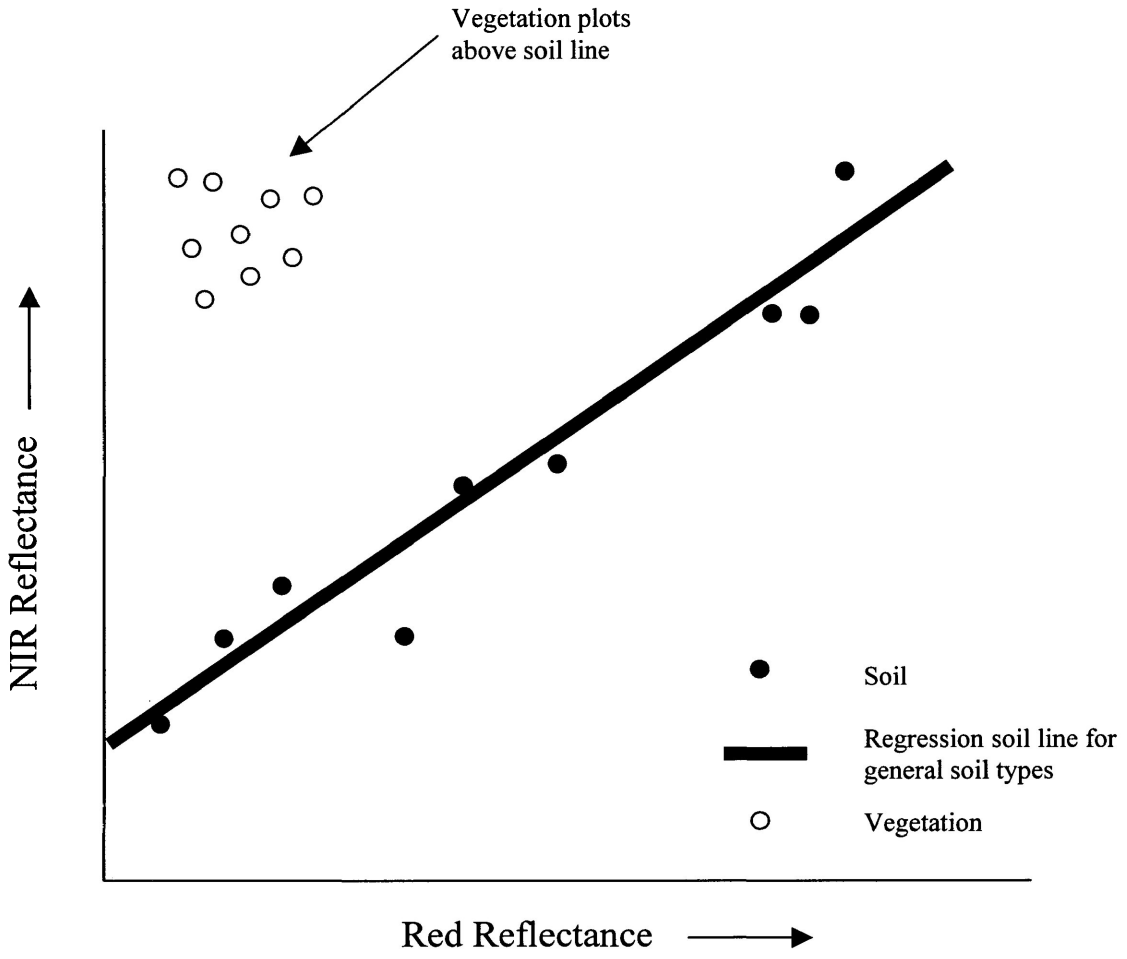


Figure 5. The soil line concept for green vegetation within R–NIR spectral coordinate space (after Richardson and Wiegand 1977).

The SAVI was developed to overcome shortfalls of the PVI, i.e., to minimize soil reflectance brightness (Huete 1988). Its use, however, is restricted to specific locations for which two constants must be experimentally calculated; thus, it is rarely used.

#### 2.2.3.3 Maximum NDVI Value Composites

A convention for reducing cloud in AVHRR imagery (e.g., Fernandez *et al.* 1997) involves the construction of *maximum value composites (MVC)* from NDVI data (Holben 1986). The MVC is obtained by first superimposing all available scenes from the compositing period to form a multi-layered image. Then, the composite image is generated by selecting the maximum value at each pixel location from the layers comprising the stack. Since clouds act to depress NDVI values, retaining the maximum values from a compositing period will provide clearer images.

Once the dates of maximum reflectance for each pixel are known for the composite period, R and NIR composites are also generated with pixel values from the equivalent dates. Viovy *et al.* (1992) compared MVC values with a competing alternative called the *best index slope extraction (BISE)*, which removes spurious high NDVI values but requires more effort to calculate, and therefore, is not widely used.

## 2.3 POTENTIAL GROUND-TRUTHING METHODS

The most labour-intensive method is collection of field data by observers or surveyors (e.g., Kasischke *et al.* 1993; Pozo *et al.* 1997; Eve *et al.* 1999). Airphoto interpretation

(e.g., Dodge and Bryant 1976; Ens 1987) is a cost-efficient alternative; however, the risk of human error can be high. Fernandez *et al.* (1997) used GPS-generated GIS database layers as ground truthing for fire disturbance studies in Spain, and Hopkins *et al.* (1988) relied on existing natural resources maps to assess the accuracy of forest land cover mapping in Wisconsin.

# CHAPTER 3 – METHODS

## DATA

### 3.1.1 AVHRR Imagery

The AVHRR/NDVI values (-1.0 to +1.0) are represented by pixel values from 10–210 on 1063-m × 1063-m spatial resolution, 10-day composite AVHRR imagery. Thus, each pixel value represents one-percent of the actual NDVI range (Eidenshink and Faundeen 1994). The AVHRR imagery was obtained from the NOAA polar orbiting television infrared observation satellites.

A joint research funding effort by NOAA, the European Space Agency, the U.S. Geological Survey, the National Aeronautics and Space Administration, the Commonwealth Scientific and Industrial Research Organization, and the Satellite Meteorological Center provides *local area coverage (LAC)* imagery free of charge at *http://edcwww.cr.usgs.gov/landdaac/1KM/comp10d.html* (Table 1). This Internet site has links to relevant and necessary online documentation. More extensive documentation of the AVHRR sensor characteristics is available in Rao (1987) and Kidwell (1991).

Table 1. Spectral channels of the AVHRR sensor.

| Channel | Description | Spectral Range |
|---|---|---|
| 1 | Visible red | 0.58 – 0.68 μm |
| 2 | Near IR | 0.73 – 1.10 μm |
| 3 | Middle IR | 3.55 – 3.93 μm |
| 4 | Thermal IR | 10.3 – 11.3 μm |
| 5 | Thermal IR | 11.5 – 12.5 μm |
| 6† | NDVI | N/A |

Shaded rows represent data channels used in this study.
† Calculated from channels 1 and 2.

### 3.1.2 Ground-Truthed Data

For the current study, ground-truthed data for testing the accuracy of fire mapping with AVHRR/NDVI consisted of a fire-pattern GIS database describing the dates and locations for fires in Ontario between 1921 and 1995 (Perera *et al.* 1998). It was compiled from hardcopy maps derived from field data, aerial photographs and interpretation of Landsat images. Lake and province boundary GIS databases were used to geo-correct AVHRR imagery.

## 3.2 DATA MANIPULATION

### 3.2.1 Threshold Methods

Decreases in AVHRR/NDVI have been used to map vegetation senescence and forest fire disturbances in various biomes (e.g., Razafimpanilo *et al.* 1995; Fernandez *et al.* 1997). Change-detection methods subtract values between two spatially complementary images and apply a threshold (Lunetta and Elvidge 1998) for discriminating significant decreases in vegetation greenness (e.g., Kasischke *et al.* 1993; Kasischke and French 1995). These methods have been established in boreal Alaska for fire disturbance mapping with NDVI data (Table 2); change values exceeding the thresholds are mapped as fires.

Threshold methods $X_1$ and $X_2$ were procedurally identical (Figure 6); only the threshold value differed. Method $X_3$ differed from the first two methods because it combined the results of two threshold values (Figure 7).

Table 2. Descriptions and references for existing AVHRR/NDVI threshold methods compared in this study.

| Threshold Method | Threshold Value (AVHRR/NDVI units) | Reference |
|---|---|---|
| $X_1$ | 23 | Kasischke *et al.* (1993) |
| $X_2$ | 24 | Kasischke *et al.* (1993) |
| $X_3$ | 23 and 18 combined | Kasischke and French (1995) |

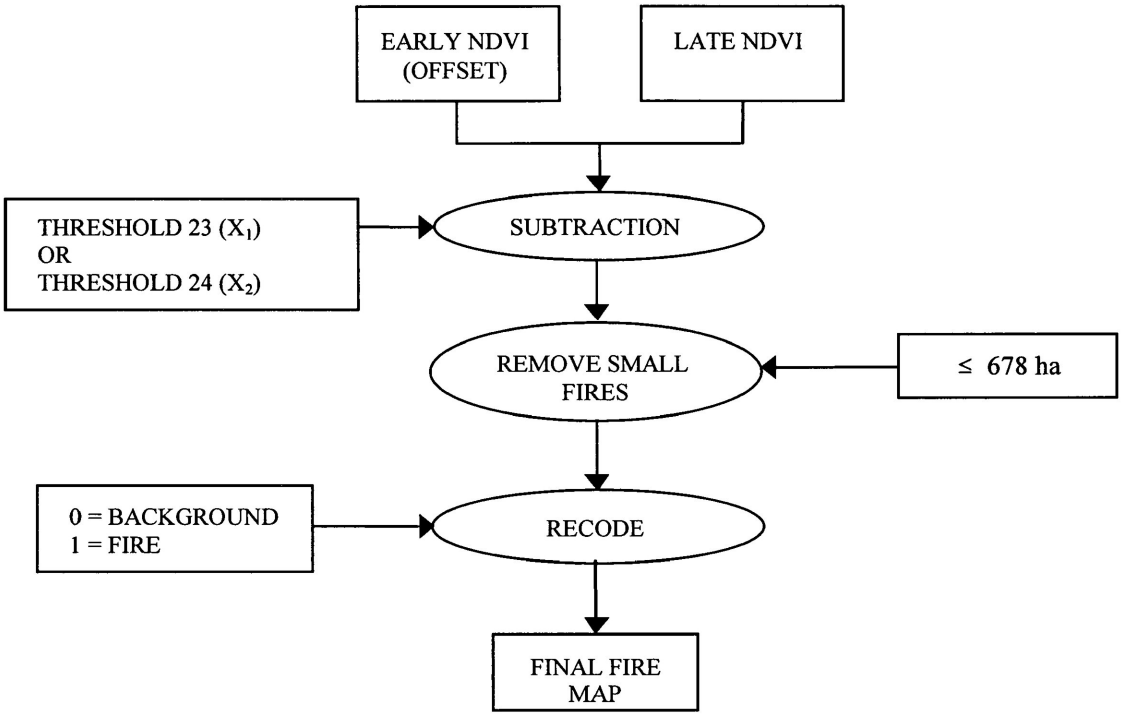


Figure 6. Processing sequence for two single-threshold methods ($X_1$ and $X_2$) to generate final fire maps from NDVI imagery. This process uses a threshold value of 23 NDVI pixel values for the $X_1$ method, and 24 for the $X_2$ method.

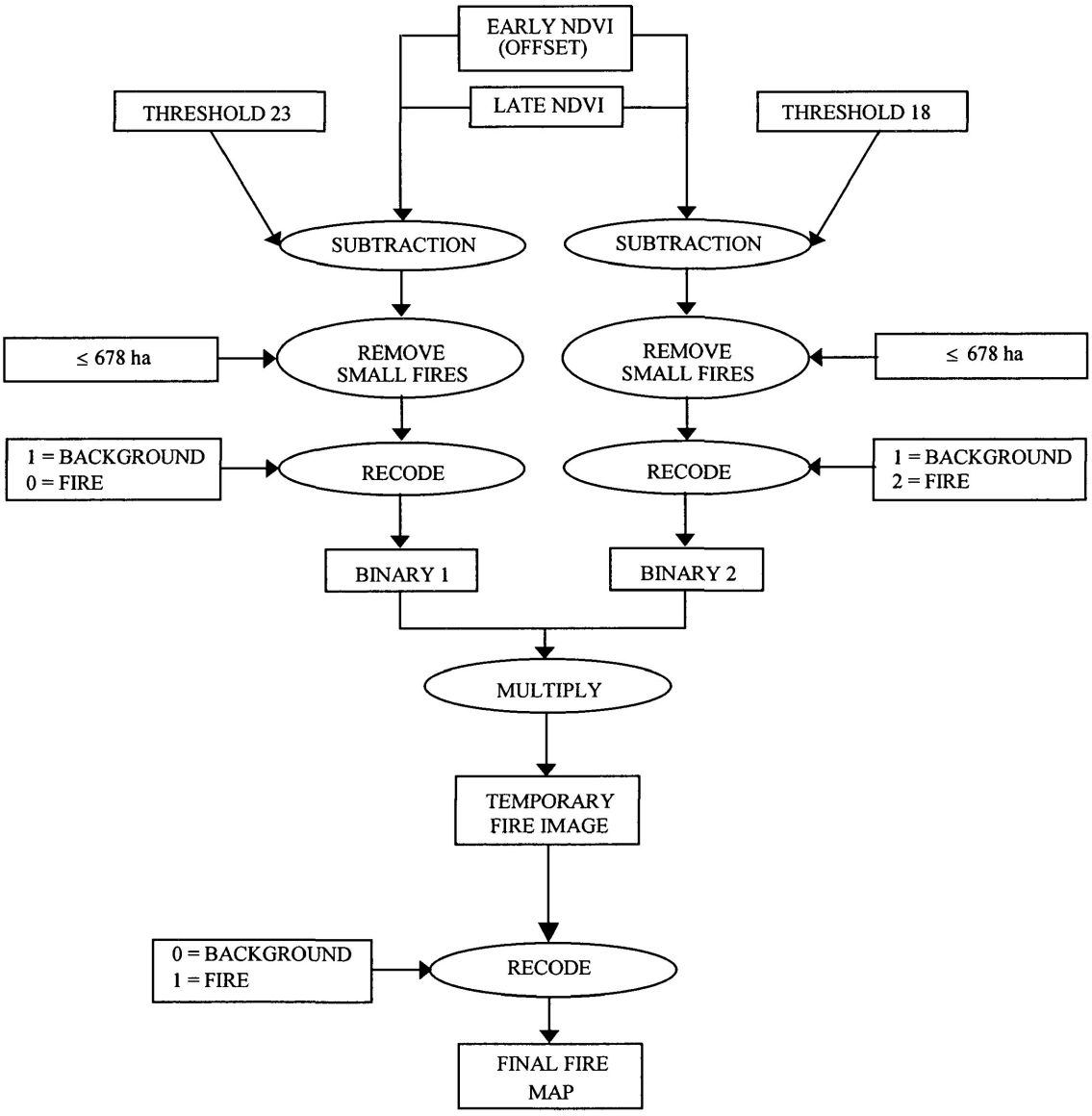


Figure 7. Processing sequence for the double-threshold method ($X_3$) to generate a final fire map from NDVI imagery. The double-threshold method ($X_3$) merges two single-threshold-generated fire maps. The first single-threshold image uses a threshold of 23 NDVI pixel units; the second uses 18.

Each threshold method required the selection of relatively cloud-free images acquired early and late during each fire season. The images were normalized to each other using an offset value (Kasischke and French 1995). For each pair of seasonal NDVI images, the late image pixel values were subtracted from those of the early images, quantifying the NDVI change. Resulting pixel values exceeding the threshold were coded as fires; the rest of the image was coded as background. Mapped fires smaller than 678 ha (six contiguous pixels) were considered noise and eliminated from analysis. This process was completed for $X_1$ and $X_2$, resulting in a set of final, binary fire maps (0s for background, 1s for fires).

Method $X_3$ generated two binary fire images, comparable to the final fire images of methods $X_1$ and $X_2$. The combination of fire pixels from two threshold values could fill spatial gaps in fire events mapped by a single threshold. The two binary images were re-coded (Figure 7) and multiplied to generate a temporary fire image, with 0s for original fires, 1s for background, and 2s for potential additions to the original fires. Then, a 7×7 focal-minimum function (ERDAS Inc. 1997) was applied to the temporary fire image (Figure 8). This function preserved original fires (0s) and potential fire pixels (2s) that were within the 7×7 focal neighbourhood of original fires. The resulting images were then re-coded to match final fire maps of methods $X_1$ and $X_2$.

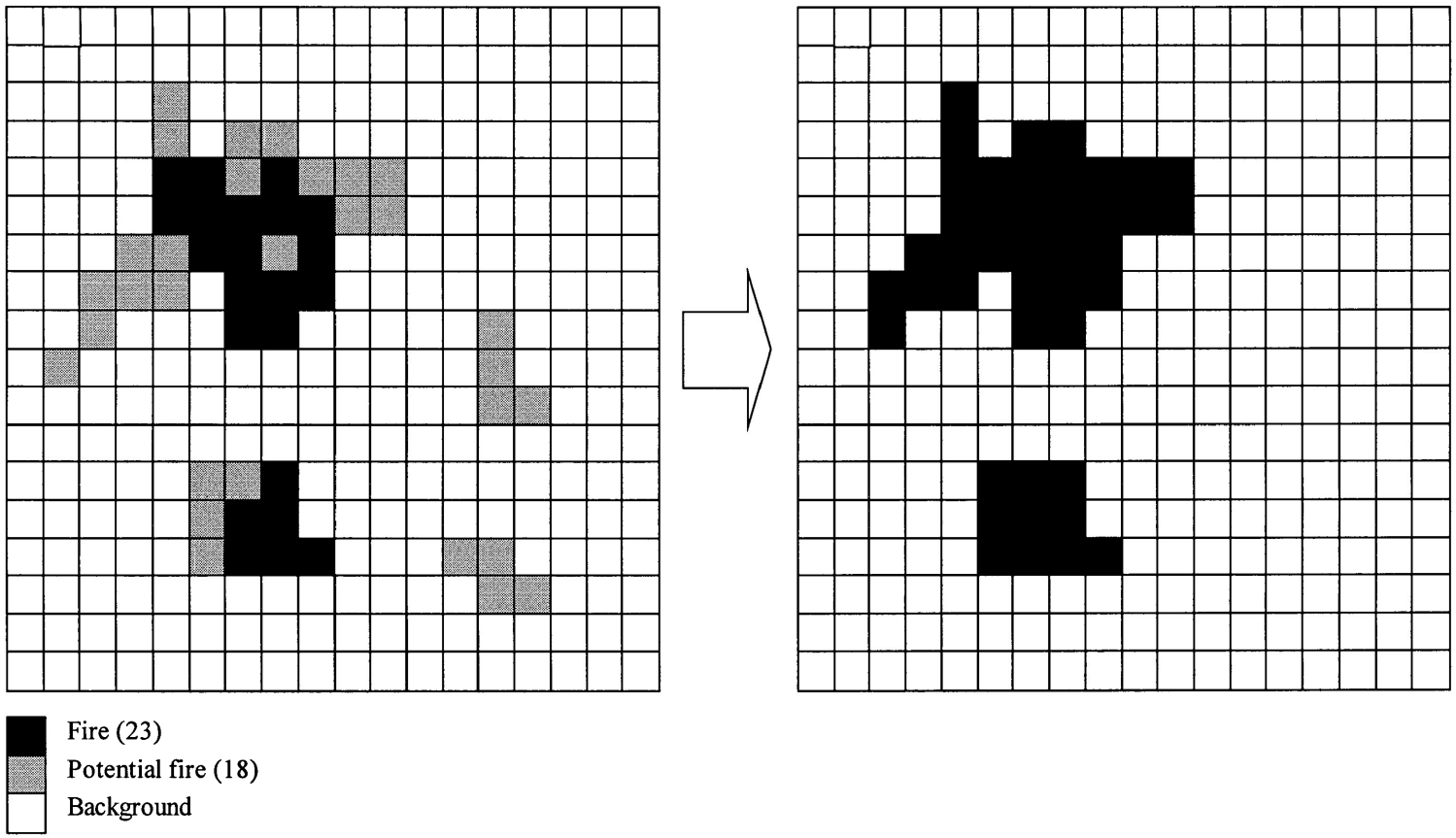


Figure 8. Example of how the double-threshold method ($X_3$) transforms potential fires within a three-pixel distance of actual fires to represent a complete fire event.

To allow each contiguous cluster larger than six pixels (mapped fire event) to be analyzed independently, the fire images were clumped (ERDAS Inc. 1997), and each cluster was numbered with a unique *grid code*.

### 3.2.2 Substrate Corrections

Substrate corrections are necessary because where canopies are not closed, particularly in burned areas, the sensor is influenced by understory and ground-level materials (Huete 1988). Therefore, two substrate corrections were proposed, and were applied to the NDVI images before change detection analysis with thresholds.

The characteristic difference between R and NIR reflectance for green vegetation has been documented and studied (e.g., Tucker 1979; Filella and Peñuelas 1994). This difference is much smaller for general soil types over the same spectral regions (e.g., Condit 1970; Stoner and Baumgardner 1981). Since both vegetation and soil reflect less in the R than NIR, their spectral curves can appear to have the same general shape if viewed only in these two broad spectral regions. To help distinguish soils from vegetation, the difference ($\Delta$) between NIR and R reflectance is important, as is the magnitude of R, which is generally much lower for vegetation than soil.

Rearranging the NDVI equation yields an opportunity to examine the influences of R magnitude and $\Delta$ on the calculation of NDVI:

$$NDVI = \Delta/(2R+\Delta) \qquad (2)$$

Similarly, this three-component relationship can be plotted as a surface (Figure 9). The NDVI surface is contained by three axes ($x$, $y$, $z$). The $x$-axis represents a gradient of all R ($10 \leq R \leq 1010$) values. The $y$-axis represents $\Delta$ ($0 \leq \Delta \leq 2000$), and the $z$-axis, the actual NDVI value calculated from Equation 2. Within these constraints, highest NDVI (as expected) is observed where R is lowest, and $\Delta$ is greatest, clearly mimicking the spectral curve of green vegetation. Conversely, lowest NDVI is seen where R is high and $\Delta$ is lowest, imitating the spectral curve of common soil types.

Superimposing the soil line (Huete and Tucker 1991) onto the surface in Figure 9 allows the definition of two dominant regions: vegetation above the soil line and non-vegetation below. This three-dimensional soil line extends from minimum NIR (where $\Delta$ is small) and R values to their maximums. Similar to Richardson and Wiegand's (1977) PVI, a gradient of increasing greenness forms from the soil line towards maximum NDVI values (low R, large $\Delta$).

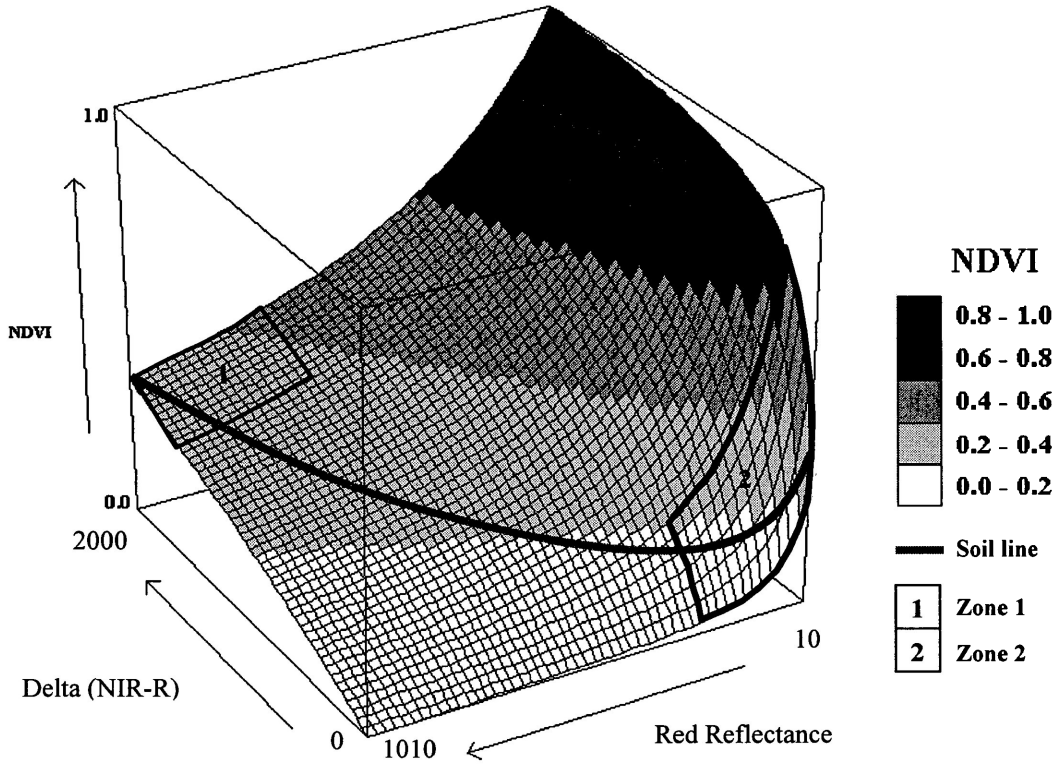


Figure 9. NDVI surface defined by R and Δ (NIR-R) components. Superimposed are the soil line (Richardson and Wiegand 1977; Huete and Tucker 1991) and two zones believed to contain falsely heightened NDVI values based on knowledge about soil and vegetation spectral reflectance patterns in the R and NIR regions of the electromagnetic spectrum.

Two areas of the NDVI/R/Δ surface (Figure 9) exhibit questionably high NDVI values given knowledge of soil and vegetation reflectance patterns in the R and NIR regions of the electromagnetic spectrum, thus warranting NDVI suppression. The exact extent and shape of the areas are not known; however, their estimated locations are marked as zones 1 and 2 in Figure 9. Zones 1 and 2 were designated rectangular (for simplicity of calculation), with dimensions governed by percentage lengths of respective bounding NDVI/R/Δ surface axes. Three variations of size (0, 10, and 15 %) were used to designate the correction effect zones $C_0$, $C_1$, and $C_2$, respectively. Since $C_0$ contains no area, it represented the uncorrected (null) effect. Zone dimensions were selected by examining R and NIR pixel distributions together with the ability of each zone to cover sufficient areas of concern on the NDVI/R/Δ surface. NDVI pixel values are considered to reside within Zone 1, with axis length $x$, when:

$$[R \leq (1000x + 10)] \text{ and } [\Delta \leq (2000x + 10)] \quad (3)$$

and Zone 2 when:

$$[R \geq (1000(1-x) + 10)] \text{ and } [\Delta \geq (2000(1-x) + 10)] \quad (4)$$

Pixel values residing within either Zone 1 or 2, for correction effects $C_1$ or $C_2$, were considered to have questionably high vegetative status and were corrected by subtracting 0.1 true NDVI units in each case (10 pixel values). The correction reduced the magnitude of greenness where R and NIR reflectances were not normal for vegetation that is green.

### 3.2.3 Geocorrecting Imagery

The mapped fire images were re-sampled to 531.5-m resolution and geo-corrected to match the projection of the GIS ground-truthing data. The increased resolution ensured a smoother fire boundary after the second-order geo-correction with nearest neighbour re-sampling (ERDAS Inc. 1997). Twenty-one ground control points were selected along distinctive hydrological features (e.g., shorelines, islands, rivers, and coastlines) (Martín and Chuvieco 1995), yielding an acceptable root mean square (RMS) error of approximately 400 m (Martín and Chuvieco 1995; Lunetta and Elvidge 1998).

### 3.2.4 Manipulation of Ground-Truthing Database

Fire polygons within the ground-truthing database (Perera *et al.* 1998) often abutted or were adjacent to other polygons, forming clusters. Thus, all polygons within 1063 m (one AVHRR pixel dimension) of each other were coded to indicate they are a part of a common ground-truthing fire *event*. To remove potential effects of varying map scale among fire *events*, the ground-truthing database was rasterized to the same resolution as the mapped fires (531.5 m) and converted back to vector format, allowing direct area comparisons.

### 3.2.5 Generating Accuracy Measures

For each treatment, the geometric unions between detected fires and the ground-truthing database were computed using ArcInfo (ESRI Inc. 1997). Overlapping polygons were split and given attributes from both original polygons. The original polygonal structures remained available by querying with original polygon identifiers (i.e., *event* and *grid code*).

Accuracy was examined from three perspectives (i.e., *sensor*, *event*, and *truth*) for each treatment. These accuracy comparisons were conducted at two levels. First, each treatment was summarized in its entirety using total truthed and detected area values. Second, individual, detected fire events (ANOVA) were compared in detail. The *sensor* perspective was omitted from the ANOVA because undetected and falsely detected fires could not be assigned to individual fire *events*. The data hierarchy and terms used to describe the structure of the union database are displayed in Figure 10.

Accuracy was assessed by calculating various measures for each treatment. These measures are described using an "ideal" database structure (Figure 11) as reference to Table 3, which lists the various measures computed.

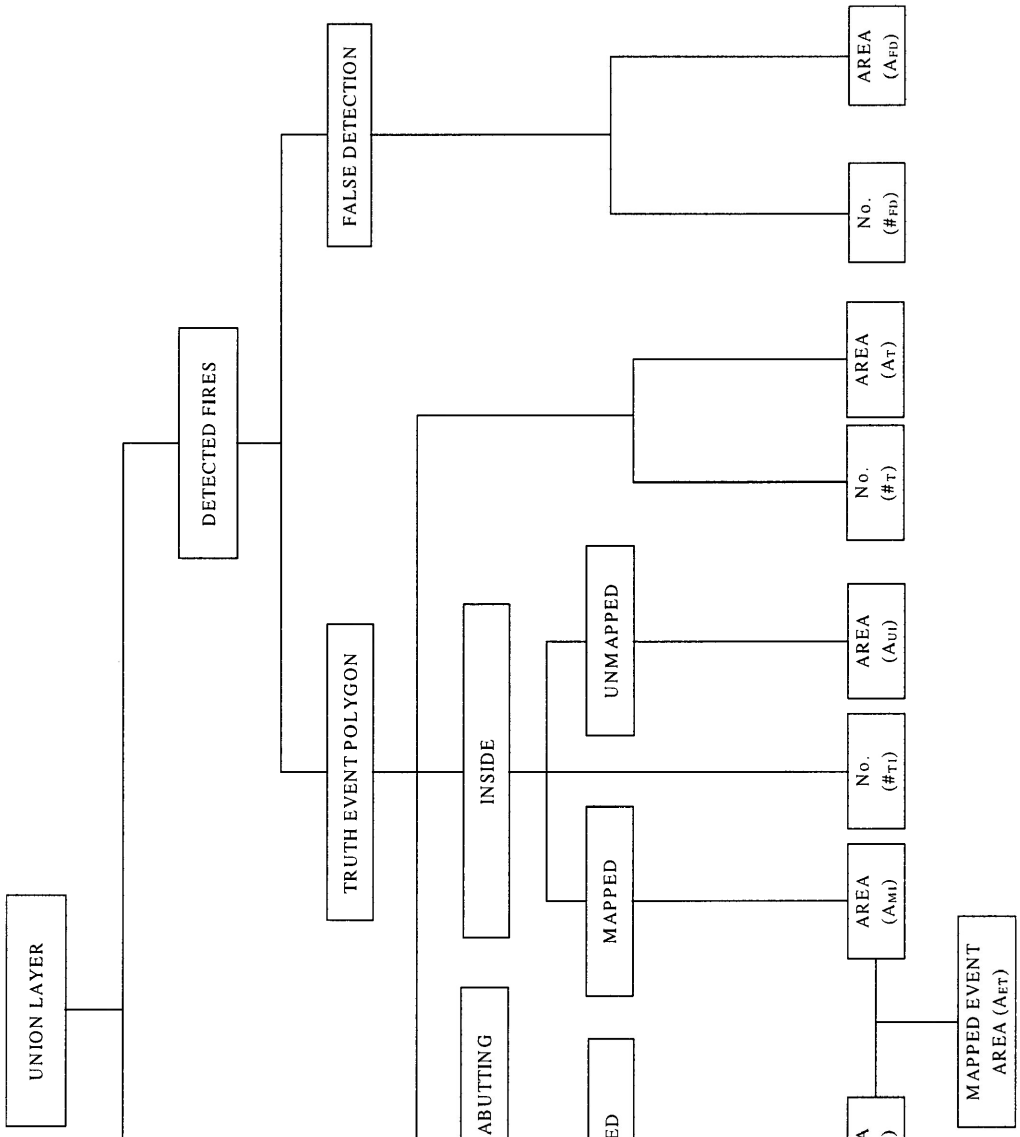


Figure 10. Hierarchical structure for the standardized naming convention (with short forms) used in this study. The union layer was generated by the geometric union of mapped and ground-truthing fire databases. The naming convention is based on occurrence numbers (#) and associated areas (A) for all possible conditions within the data hierarchy. Subscripts denote the specific branch within the hierarchy, using combinations of letters designating higher hierarchical levels to represent the end condition.

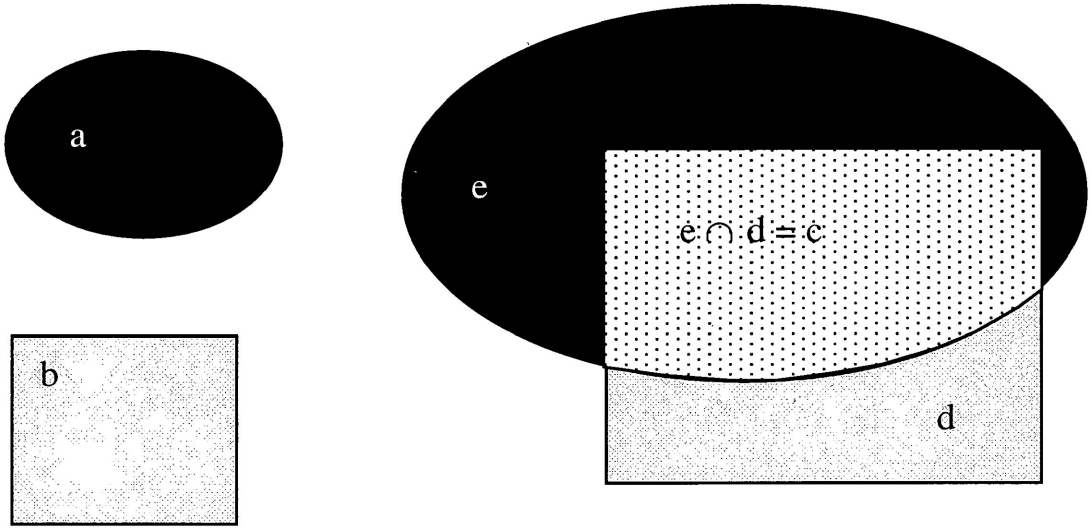


Figure 11. Resulting components of the computed geometric union between mapped/detected fires and ground-truthing fires. Mapped/detected fires (rectangle) and truthing fires (oval): (a) undetected fire, (b) falsely detected fire, (c) area mapped inside ground-truthing perimeters, (d) mapped fire outside ground-truthing perimeters, and (e) unmapped area inside ground-truthing perimeters.

Table 3. Perspectives, observation levels, accuracy measures, and calculations for summarizing fire mapping accuracy.

| Perspective | Level | Name | Accuracy Measure* | Calculation† |
|---|---|---|---|---|
| Sensor | General | Correct | $A_{MI} / (A_{ET} + A_{FD})$ | c / (b + c + d) |
| | | Incorrect | $(A_{MO} + A_{FD})/(A_{ET} + A_{FD})$ | (b + d) / (b + c + d) |
| | | Omission | $(A_{UI} + A_{UD})/(A_{ET} + A_{FD})$ | (e + a) / (b + c + d) |
| Event | General | Correct | $A_{MI} / A_{ET}$ | c / (c + d) |
| | | Incorrect | $(A_{MO} + A_{FD}) / A_{ET}$ | (b + d) / (c + d) |
| | | Omission | $(A_{UI} + A_{UD}) / A_{ET}$ | (e + a) / (c + d) |
| | Detailed | Correct | $A_{MI} / A_{ET}$ | c / (c + d) |
| | | Outside | $A_{MO} / A_{ET}$ | d / (c + d) |
| | | Omission | $A_{UI} / A_{ET}$ | e / (c + d) |
| Truth | General | Correct | $A_{MI} / A_T$ | c / (a + c + e) |
| | | Incorrect | $(A_{MO} + A_{FD}) / A_T$ | (b + d) / (a + c + e) |
| | | Omission | $(A_{UI} + A_{UD}) / A_T$ | (e + a) / (a + c + e) |
| | Detailed | Total | $A_{ET} / A_T$ | (c + d) / (c + e) |
| | | Correct | $A_{MI} / A_T$ | c / (c + e) |
| | | Outside | $A_{MO} / A_T$ | d / (c + e) |

* Nomenclature is derived from the hierarchical naming convention established in Figure 10.
† Example calculation areas are established in Figure 11.
Shaded cells represent dependent (response) variables entered into the ANOVA.
Components: ($A_{MI}$) area mapped inside ground-truthing perimeters, ($A_{ET}$) area of total mapped event, ($A_{FD}$) area falsely detected, ($A_{MO}$) area mapped outside ground-truthing perimeters, ($A_{UI}$) area unmapped inside ground-truthing perimeters, ($A_T$) area of total ground-truthing fire, and ($A_{UD}$) area of ground-truthing fires undetected.

## EXPERIMENTAL DESIGN

### 3.3.1 Treatment Design

Three change-detection techniques utilizing NDVI thresholds for fire mapping form the base methods for data processing ($X_1$, $X_2$, and $X_3$). Before threshold processing, three levels of substrate corrections ($C_0$, $C_1$, and $C_2$) are applied to the NDVI imagery. These combinations were repeated for fire years 1992, 1993, and 1995 ($Y_k$). Therefore, 27 treatments (unique combinations of three fire years, three threshold methods, and three substrate corrections) were established, for which measured accuracy response variables were computed (Figure 12).

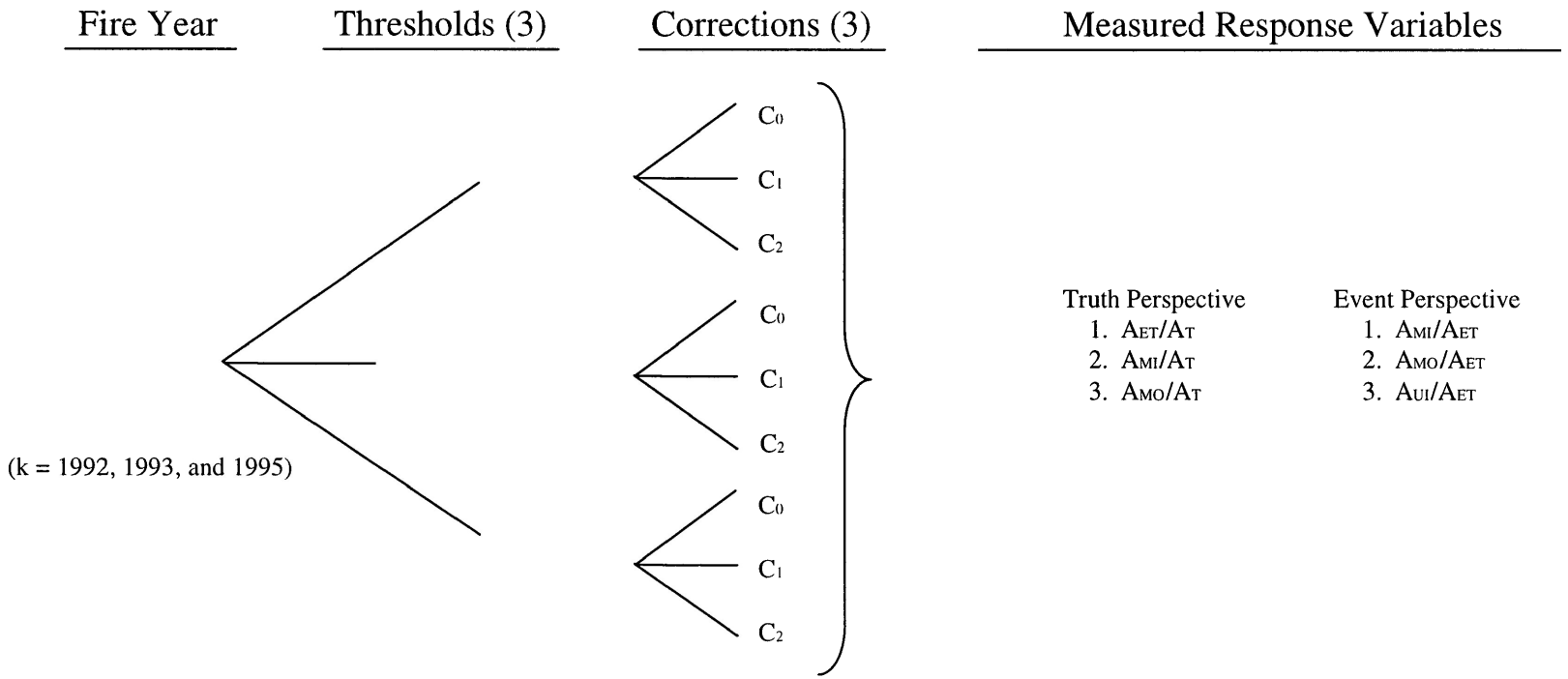


Figure 12. 3×3 factorial treatment structure for years 1992, 1993, and 1995. Fire years are represented by ($Y_k$): 1992, 1993, and 1995. ($X_1$) and ($X_2$) are single-threshold methods and ($X_3$) is the double-threshold method. ($C_0$) represents no substrate correction, ($C_1$) slight substrate correction, and ($C_2$) highest substrate correction administered in this study. Variable components: ($A_{ET}$) area of total mapped fire event, ($A_T$) area of ground-truthing fire, ($A_{MI}$) area mapped inside ground-truthing perimeters, ($A_{MO}$) area mapped outside ground-truthing perimeters, and ($A_{UI}$) area unmapped inside ground-truthing perimeters.

### 3.3.2 Statistical Design

A 3×3 factorial ANOVA (SPSS 1997) design was used to test the null hypotheses for the fixed substrate corrections (i.e., $C_0$, $C_1$, and $C_2$) and fixed threshold methods (i.e., $X_1$, $X_2$, and $X_3$). Tests of significance ($\propto = 0.05$) were conducted separately for each fire season (1992, 1993, and 1995). The model was unbalanced because the natural processes could not ensure an equal number of cases in each treatment. Data normality (an assumption of ANOVA) was ensured by re-scaling the percent-type accuracy variables to proportions and transformed using the arcsine-square-root function.

Six ratio-scale variables (Figure 12) were tested separately within this statistical design, three each from the *event* and *truth* perspectives. Variables calculated from the *event* perspective are based on the total area associated with each ground-truthing *event*, and the *truth* perspective is based on the area of ground-truthing fires (Kasischke and French 1995). Significant differences were tested with Scheffé's post hoc tests ($\propto = 0.05$) using harmonic means (SPSS 1997) to determine which effects differed within factors. Scheffé's test was selected due to its conservative nature and ability to make linear comparisons between effects, instead of conducting all pair-wise comparisons.

### 3.3.3 Statistical hypotheses

Given the goals and objectives outlined in the introduction, the following hypotheses were tested for each of the six accuracy variables computed in this study (Figure 12):

Test equality among three substrate correction effects:
$H_o$: $\mu_{\tau 1} = \mu_{\tau 2} = \mu_{\tau 3} = 0$
$H_1$: at least one $\mu_{\tau i} \neq 0$

Test equality among three threshold method effects:
$H_o$: $\mu_{\beta 0} = \mu_{\beta 1} = \mu_{\beta 2} = 0$
$H_1$: at least one $\mu_{\beta i} \neq 0$

Test interaction among threshold methods and substrate corrections:
$H_o$: $(\mu_\tau \mu_\beta)_{ij} = 0$ (for all effects of i and j)
$H_1$: at least one $(\mu_\tau \mu_\beta)_{ij} \neq 0$

The linear notation of the ANOVA model:

$$y_{ijk} = \mu + \tau_i + \beta_j + (\tau\beta)_{ij} + \in_{ijk}$$

$y$ = observation
$\mu$ = grand-mean effect
$\tau$ = effect of substrate correction
$\beta$ = effect of threshold method
$\in$ = error associated with observation

# CHAPTER 4 – RESULTS AND DISCUSSION

The results and associated discussions are separated into two broad classes: 1) general overview of treatment totals (*sensor*, *event*, and *truth* perspectives) and 2) detailed comparison of areal coincidence for detected fires (*event* and *truth* perspectives). Discussion of detected fire numbers and their respective areas are included with the general overview of treatments.

## GENERAL OVERVIEW OF TREATMENT TOTALS

### 4.1.1 Comparing General Fire Numbers

The number of ground-truthed fires and the total area burned varied among fire years (Table 4). Charting the percentage of correctly detected fires, along with those falsely detected (Figure 13), provides a summary of detection successes and errors (commission and omissions) for each treatment.

Table 4. Occurrence and area disturbed by forest fires in Ontario during study period.

| | Fires in Truthing Database | |
|---|---|---|
| Year | Number | Total Area* |
| 1992 | 12 | 151 900 |
| 1993 | 10 | 70 700 |
| 1995 | 34 | 325 900 |

* Areas are rounded to the nearest 100 ha.
Source: Ground-truthing database (Perera *et al*. 1998).

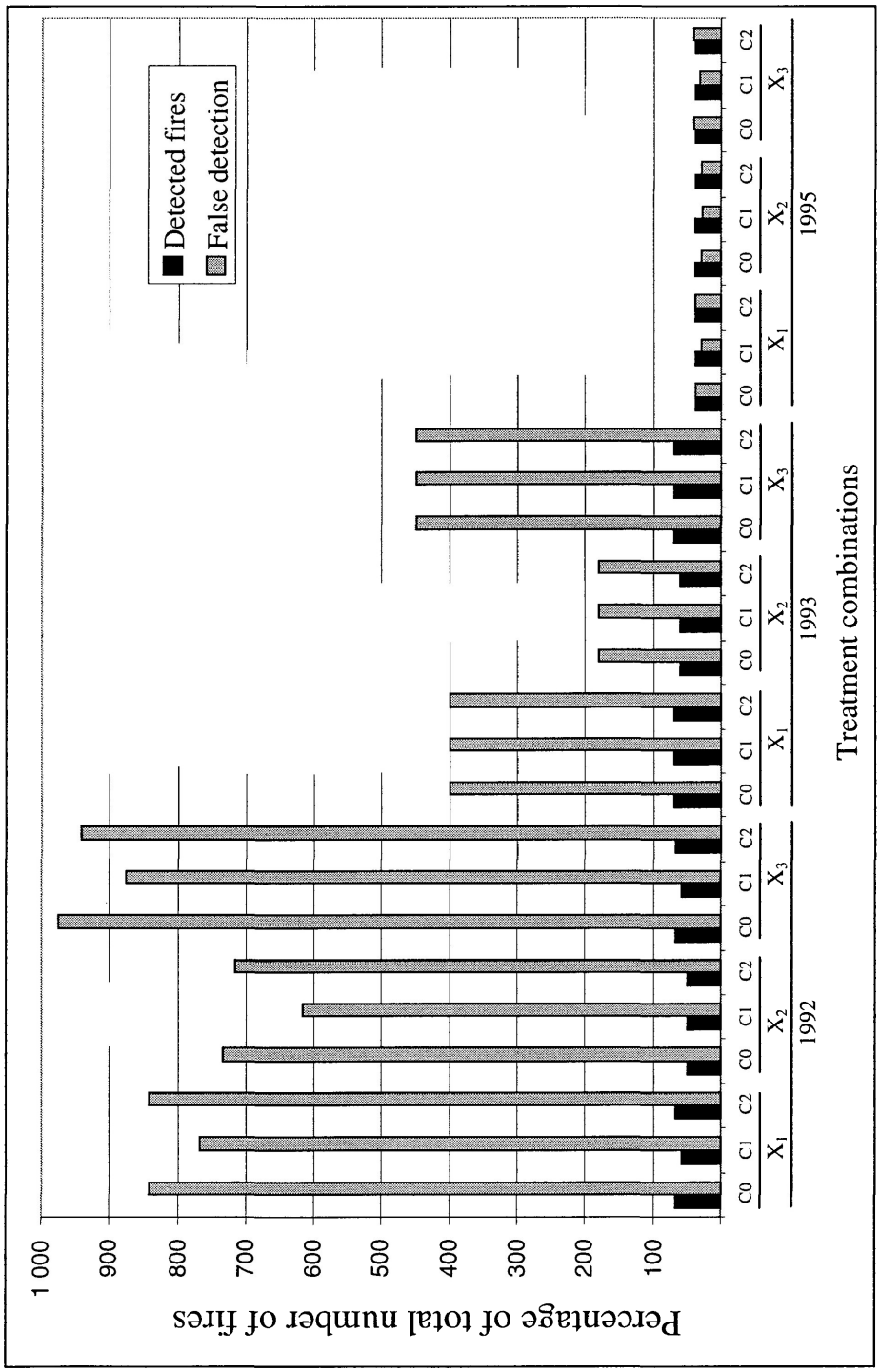


Figure 13. Percentage of correctly and falsely detected fire events in relation to the datum of ground-truthing fires in each treatment. Omissions are represented by the difference between detected fires the 100% datum. ($X_1$ and $X_2$) represent single threshold methods, ($X_3$) double threshold method, ($C_0$) no substrate correction, ($C_1$) slight substrate correction, and ($C_2$) high substrate correction.

Average false-detection percentages were highest in 1992 (812%), intermediate in 1993 (343%), and lowest in 1995 (34%) (Figure 13). Incidences of false detection were significantly higher in 1992 ($n = 27$, $p < 0.05$) than either 1993 or 1995, indicating highest commission error. Although 1995 exhibited lowest commission error, the higher number of ground-truthed fires emphasized errors of omission due to lack of detection. Incidences of correct fire detection were significantly highest in 1993, intermediate in 1992, and lowest in 1995 ($n = 27$, $p < 0.05$). There were too few years of data to statistically test for differences among threshold methods or substrate corrections at the general treatment-level, regarding detection numbers.

Although statistical comparisons were not possible among threshold methods or substrate corrections at the general treatment level, false detection seemed to be influenced by the threshold method used. Despite magnitude changes among years, these patterns were similar for each year of study. Thus, with further study (more years of data), it should be possible to indicate which of the threshold methods statistically returns the most accurate numbers of fire detection, lowest commission, and minimal omission.

The very high occurrence of falsely detected fires in 1992 cannot be explained with certainty. However, the pattern exhibited by 1992 fires could indicate the influence of a thin cloud layer that depresses the NDVI values, classifying them as fires (e.g., Kasischke and French 1995) even though NDVI helps reduce background noise effects (Chen 1996).

### 4.1.2 Comparing General Fire Areas

The general summary of total fire area (Figure 14) indicates significant differences in false detection among years ($n = 27$, $p \geq 0.05$), with 1992 having highest occurrence. Therefore, the high numbers of false detection incidences in 1992 were substantiated by highest area of commission error. Mapped *event* area also differed among years ($n = 27$, $p < 0.05$), with 1993 and 1995 having the highest mapped event areas, approaching 100% of the ground-truthing area datum. No significant differences were found among years for areas mapped outside ground-truthing perimeters ($n = 27$, $p \geq 0.05$), but areas mapped inside increased with each consecutive year ($n = 27$, $p < 0.05$). Finally, the area unmapped (omission inside ground-truthing perimeters) was significantly lower in 1995 than in either 1992 or 1993 ($n = 27$, $p < 0.05$).

The variability of interannual fire numbers and area burned is supported by other studies (e.g., Cahoon *et al.* 1996; Martell and Boychuk 1997). However, fire numbers and areas burned do appear to be related.

Total mapped-*event* area provides a better estimate of actual fire size than does correctly mapped fire area, even when positional coincidence between a mapped fire and its corresponding ground-truthing fire areas is low. Differences in area among substrate correction effects and threshold effects were not tested because of limited replication by fire year.

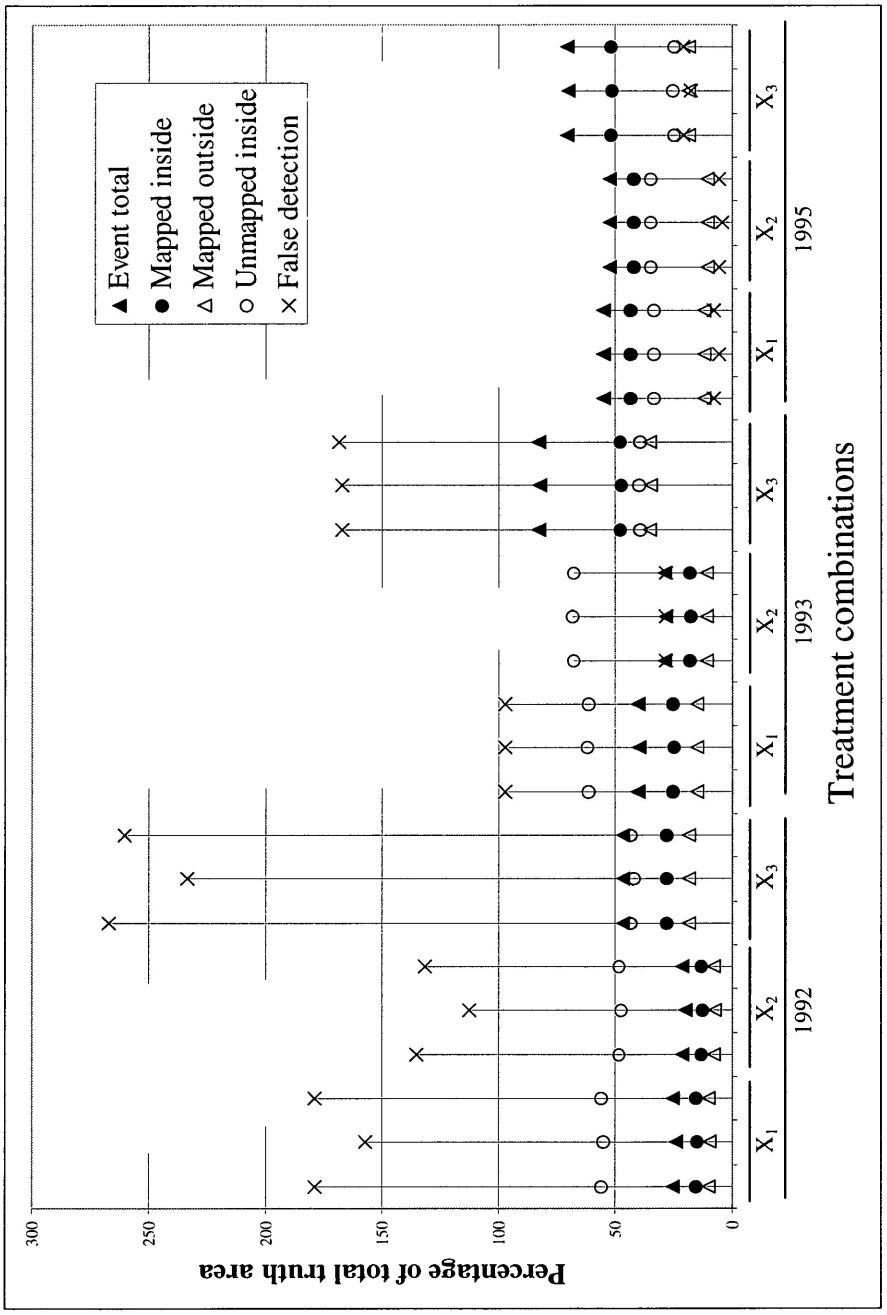


Figure 14. Percentages of areas mapped in relation to the ground-truthing fire datum area in each treatment. ($X_1$) and ($X_2$) represent single-threshold methods, ($X_3$) double threshold method, ($C_0$) no substrate correction, ($C_1$) slight substrate correction, and ($C_2$) high substrate correction.

### 4.1.3 Potential Sources of Error

During the compilation of the ground-truthing fire database, two disturbances types were omitted: those that could not be verified by two sources and fires that were not "stand destroying" (Perera *et al.* 1998). Therefore, some falsely detected fires in this study may represent omitted ground truthing. Some falsely detected fires, however, may actually represent insect infestations, drought, smoke (Pereira and Setzer 1993), or other forest stresses that produce similar spectral conditions (e.g., Murtha 1973).

The fire detection/mapping methods compared in this study tended to over-represent total fire areas, which is contrary to similar studies (e.g., Kasischke *et al.*1993; Kasischke and French 1995). The under-representation of ground-truthing fires by the Kasischke studies was explained with a citation from Cahoon *et al.* (1992) claiming that 10-day image composites exhibit bias for high NDVI values; thus, disturbances occurring late in the composite period would be omitted. Late-occurring fires would not appear on the imagery until the following composite period, or if they occurred late in the fire season, not until the following year. Such cases can lead to an increase in undetected fire numbers and associated areas (increased error of omission).

Seasonal and annual timing can alter the NDVI recorded on imagery due to differences in phenology (Kasischke and French 1997). Abscission during an early fall can contribute to patchy decreases in NDVI, potentially increasing numbers and areas of false fire detection, while a late spring could reduce initial (baseline) NDVI values.

These seasonal effects indicate the importance of timing to obtain optimal imagery for fire detection and mapping studies (e.g., Kasischke and French 1993).

Inter- and intra-annual effects could be explained due to climatic trends observed during the study period, as in Kasischke and French (1997). The 1995 fire season exhibited low precipitation (Environment Canada 1998), resulting in a high number of forest fires that burned extensive areas (Table 4). High precipitation during 1992 and 1993 (Environment Canada 1998) is reflected by both low fire numbers and area burned (Table 4).

### 4.1.4 General Fire Shapes

The mapped fire shapes were similar to those in the ground-truthing database (Figure 15). Seasonal fire patterns are shown in Figure 16. The ability to map fires accurately can be related to fire size (Kasischke *et al.* 1993), severity (White *et al.* 1996), vegetation moisture content (Patterson and Yool 1998), and level of cloud contamination (Kasischke and French 1995).

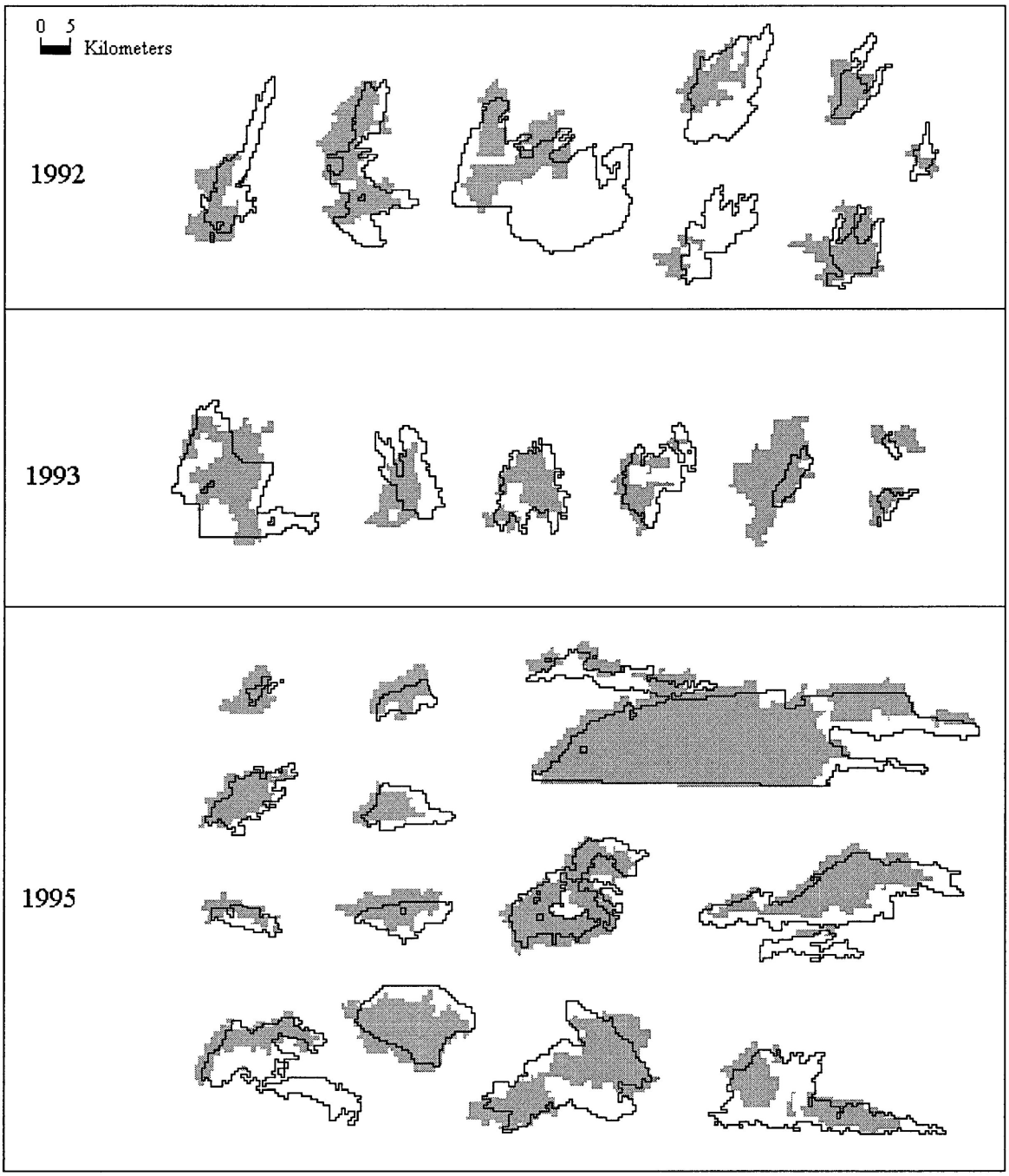


Figure 15. Comparison of area detected for each ground-truthing fire. All cases were extracted from the double threshold treatment ($X_3$) with no substrate correction ($C_0$). Shaded area represents AVHRR/NDVI mapped fire; black outline represents ground-truthing fire perimeter.

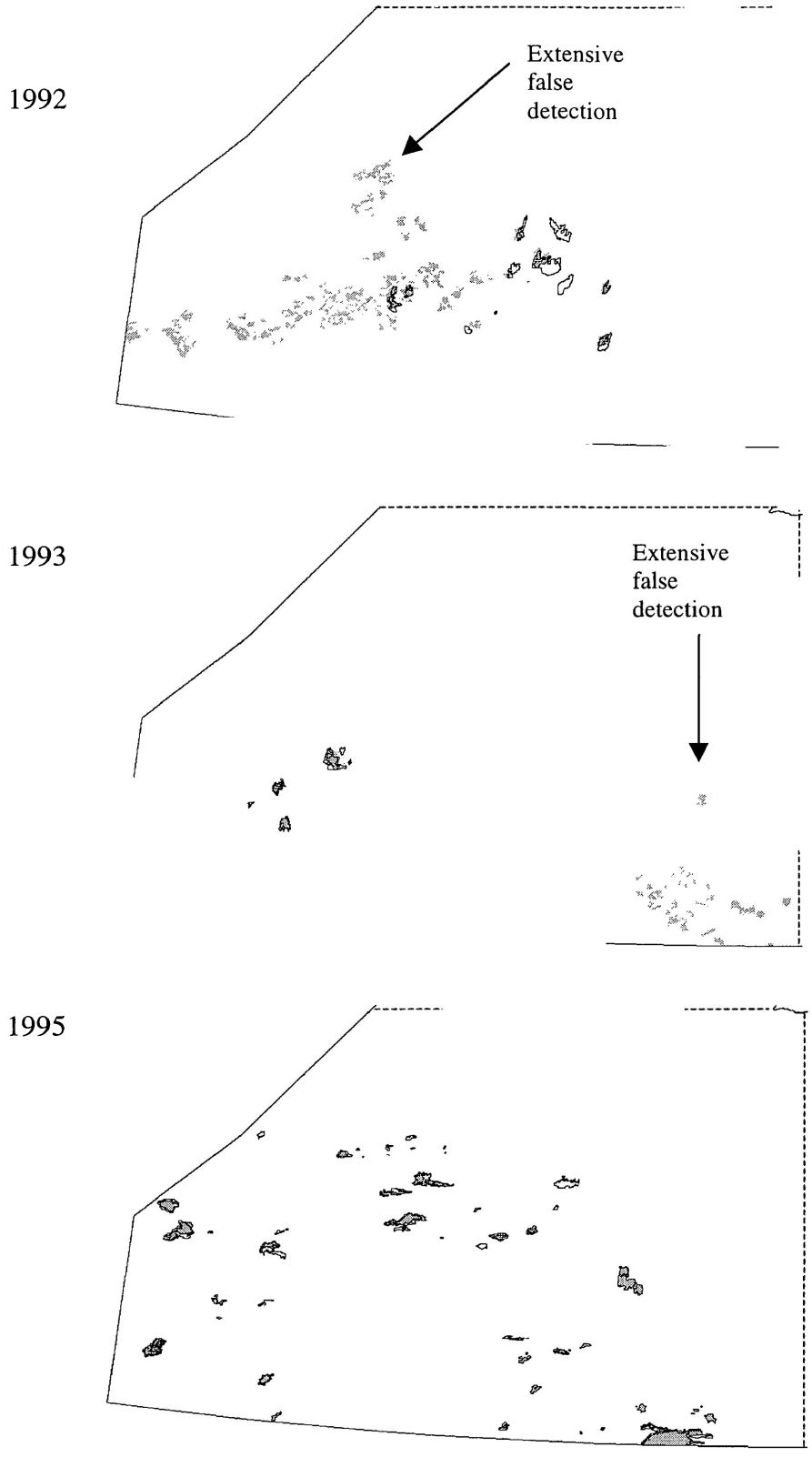


Figure 16. Fires mapped with the double-threshold method and no substrate correction for 1992, 1993, and 1995 fire seasons. AVHRR/NDVI mapped fires (shaded) with ground-truthing reference perimeters. Study area boundary is shown along southern and western boundaries; the dashed line represents where the study area was trimmed for display purposes.

Because only three years of data were analyzed, resulting in a low number of replicates, inferences are specific to the study period and cannot be extrapolated to other seasons without further sampling and study.

### 4.1.5 General Sensor Perspective – Accuracy Assessment

The accuracy levels calculated from the *sensor* perspective for all 27 treatments are displayed in Figure 17. The percentages of correctly detected fire areas differed each year ($n = 27$, $p < 0.05$), as did the percentage of area detected incorrectly ($n = 27$, $p < 0.05$). No significant differences were observed for percentage of omission area during the three years ($n = 27$, $p \geq 0.05$).

Due to limited replicates resulting from only three years of data, statistical comparisons could not be conducted among accuracy metrics for the general *sensor* perspective. However, Figure 17 suggests that omission can be reduced with the double-threshold method ($X_3$). It also suggests that incorrectly detected fires may be reduced with the strictest, single-threshold method ($X_2$) while increasing correct detection. The lower omission observed with the double-threshold method compared to the single-threshold methods was noted by Kasischke and French (1993). Negligible effects are observed for substrate corrections.

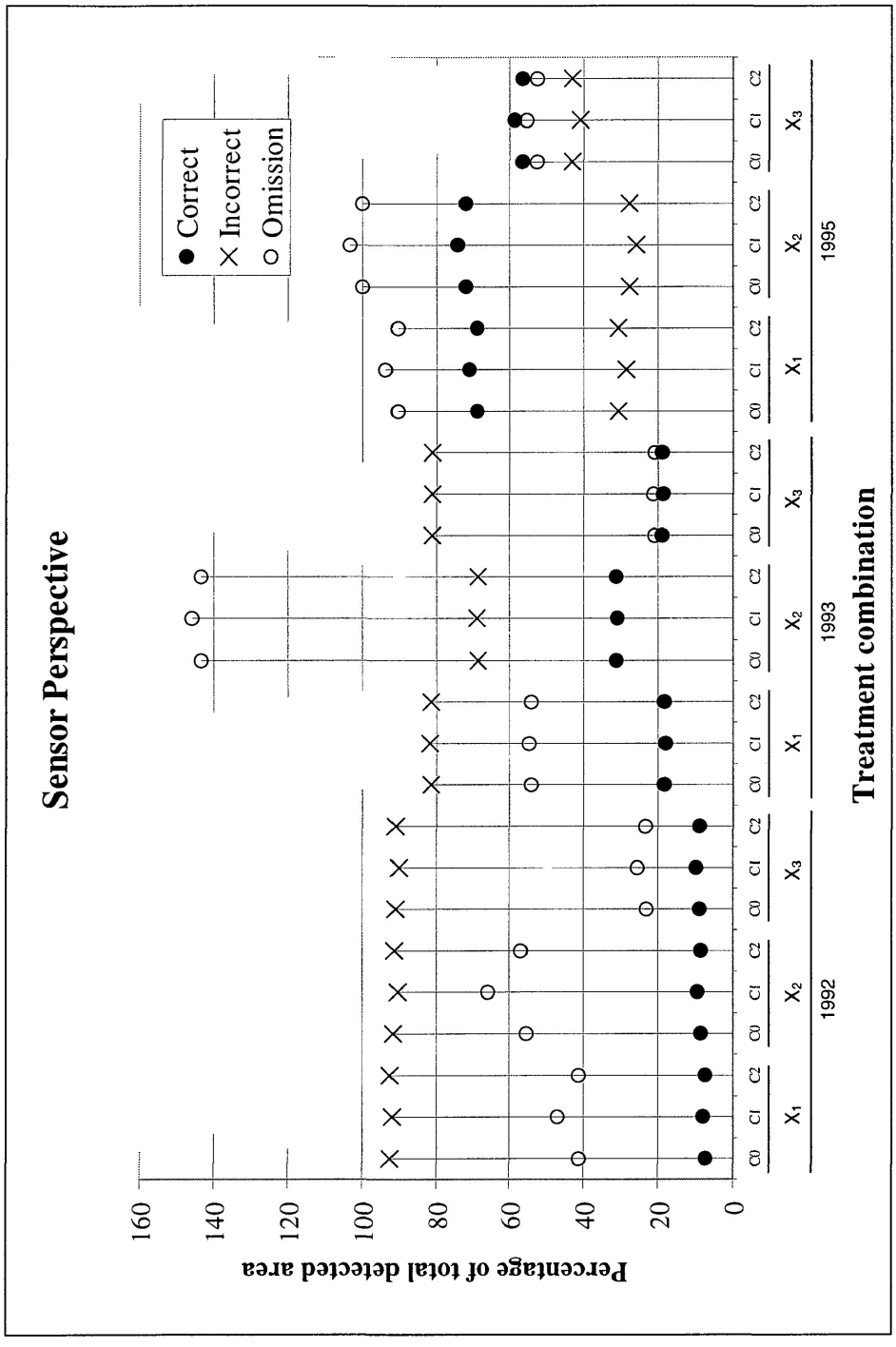


Figure 17. Comparisons of correctly, incorrectly, and undetected (omitted) area measurements among treatments from the sensor perspective. ($X_1$ and $X_2$) single-threshold methods, ($X_3$) double-threshold method, ($C_0$) no substrate correction, ($C_1$) slight substrate correction, and ($C_2$) high substrate correction.

### 4.1.6 General Event Perspective – Accuracy Assessment

The accuracy levels calculated from the *event* perspective for all 27 treatments are displayed in Figure 18. Accuracy measurements were compared with each treatment's total *event* area (i.e., areas abutting or overlapping ground-truthing *events*) as a datum. The percentage of correctly detected fire areas was highest in 1995 ($n = 27$, $p < 0.05$). The percentage of incorrectly detected fire area was highest in 1992, and lowest in 1995 ($n = 27$, $p < 0.05$). Omission was highest in 1992, with 1993 and 1995 considered statistically equal ($n = 27$, $p < 0.05$).

Due to limited replicates resulting from only three years of data, statistical comparisons could not be conducted among accuracy metrics for the general *event* perspective. However, Figure 18 suggests that omission can be reduced by using the double-threshold method ($X_3$), and incorrect detection can be reduced with the strictest threshold method ($X_2$). Negligible effects are observed for substrate corrections.

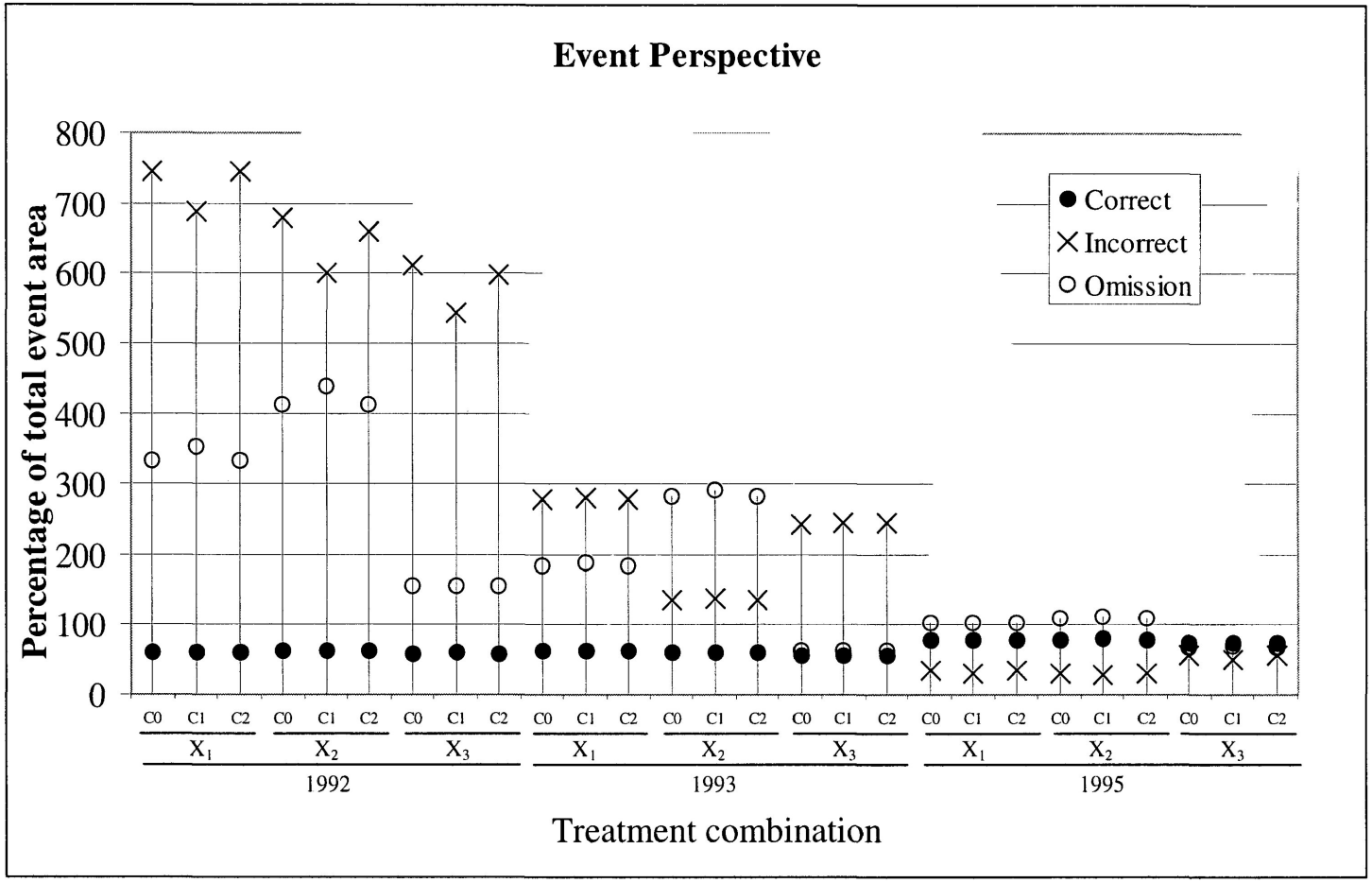


Figure 18. Comparisons of correctly, incorrectly, and undetected (omitted) area measurements among treatments from the event perspective. ($X_1$ and $X_2$) single-threshold methods, ($X_3$) double-threshold method, ($C_0$) no substrate correction, ($C_1$) slight substrate correction, and ($C_2$) high substrate correction.

### 4.1.7 General Truth Perspective – Accuracy Assessment

The accuracy levels calculated by the *truth* perspective for all 27 treatments are displayed in Figure 19. These accuracy measurements were calculated with ground-truthing fire area as the datum. Significant differences were noted for the percentage of correctly mapped fires among all years ($n = 27$, $p < 0.05$), with 1995 being the most accurate and 1992 the least. Both percentages of incorrectly mapped fire area and omission area differed significantly each year ($n = 27$, $p < 0.05$), with 1995 exhibiting lowest values and 1992 the highest.

Due to limited replicates resulting from only three years of data, statistical comparisons could not be conducted among accuracy metrics for the general *truth* perspective. However, Figure 19 suggests that the strictest single-threshold method ($X_2$) could reduce incorrect detection. Furthermore, the double-threshold method ($X_3$) appears to return highest accuracy values for correctly mapped fires. The $X_3$ method, although returning highest accuracy for mapping inside ground-truthing perimeters, also exhibits highest incorrect detection, thus making selection of an optimal method difficult. Substrate correction effects appear negligible. Table 5 summarizes the accuracy for all perspectives, years, components, and threshold methods.

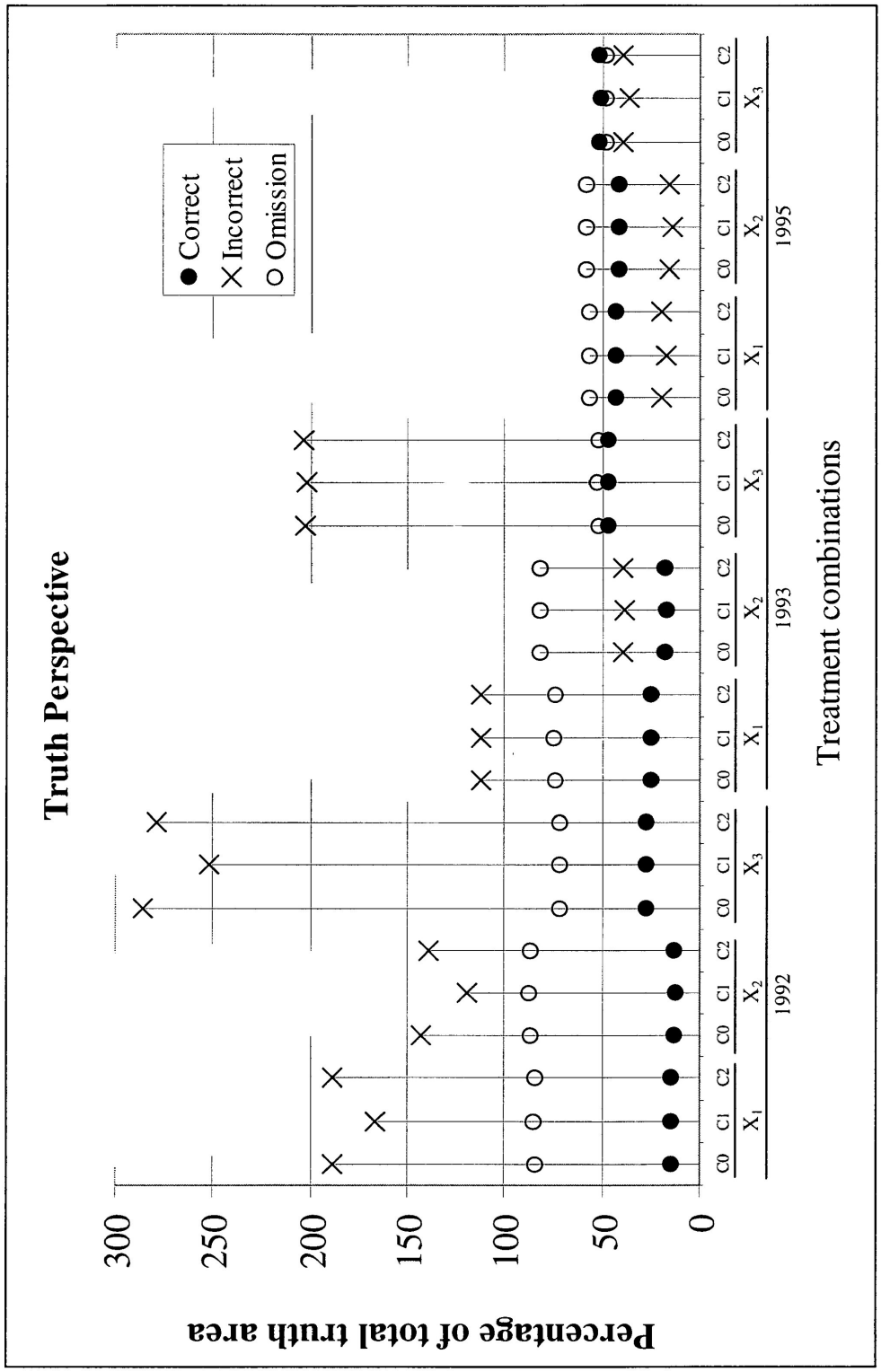


Figure 19. Comparisons of correctly, incorrectly, and undetected (omitted) area measurements among treatments from the truth perspective. Treatments: ($X_1$ and $X_2$) single-threshold methods, ($X_3$) double-threshold method, ($C_0$) no substrate correction, ($C_1$) slight substrate correction, and ($C_2$) high substrate correction.

Table 5. General treatment-level summary of accuracy.

| Method | Perspective | Component | 1992 (%) | 1993 (%) | 1995 (%) |
|---|---|---|---|---|---|
| Intermediate | Sensor | Correct | 8 | 18 | 70 |
| | | Incorrect | 92 | 82 | 30 |
| | | Omission | 43 | 54 | 92 |
| | Event | Correct | 61 | 63 | 78 |
| | | Incorrect | 727 | 279 | 34 |
| | | Omission | 340 | 186 | 103 |
| | Truth | Correct | 15 | 25 | 43 |
| | | Incorrect | 182 | 112 | 19 |
| | | Omission | 85 | 75 | 57 |
| Strict | Sensor | Correct | 9 | 31 | 73 |
| | | Incorrect | 91 | 69 | 27 |
| | | Omission | 59 | 144 | 101 |
| | Event | Correct | 63 | 62 | 80 |
| | | Incorrect | 647 | 136 | 30 |
| | | Omission | 421 | 286 | 111 |
| | Truth | Correct | 13 | 18 | 42 |
| | | Incorrect | 134 | 39 | 16 |
| | | Omission | 87 | 82 | 58 |
| Lenient | Sensor | Correct | 9 | 19 | 57 |
| | | Incorrect | 91 | 81 | 43 |
| | | Omission | 24 | 21 | 54 |
| | Event | Correct | 60 | 58 | 74 |
| | | Incorrect | 585 | 245 | 55 |
| | | Omission | 155 | 64 | 69 |
| | Truth | Correct | 28 | 48 | 52 |
| | | Incorrect | 272 | 203 | 38 |
| | | Omission | 72 | 52 | 48 |

## 4.2 DETAILED MAPPING ACCURACY COMPARISONS

Total *event* area ($A_{ET}$) and total ground-truthing area ($A_T$), along with areas mapped inside ($A_{MI}$), and outside ($A_{MO}$) ground-truthing perimeters, were required to calculate the suite of accuracy measures defined in the *Methods*. Since these values cannot be calculated for false detection ($A_{FD}$) or undetected fires ($A_{UD}$), detailed accuracy comparisons were completed only for detected fires. Results and discussion regarding mapping accuracy between treatments at a fire-by-fire level are in the following two sections: 1) from the *truth* perspective and 2) from the *event* perspective.

### 4.2.1 Truth Perspective

For the *truth* perspective, the ANOVA tests (Table 6) found no significant differences ($p \geq 0.05$) among substrate correction effects or interaction effects among threshold methods and substrate corrections. However, significant differences ($p < 0.05$) were found among threshold methods in each year and for all accuracy measures, except for the area mapped outside truthing perimeters ($A_{MO}/A_T$) in 1993. Therefore, the null hypotheses for substrate correction could not be rejected. Null hypotheses were rejected for all threshold methods except $A_{MO}/A_T$ (1993). Since no significant interactions were observed among threshold and correction factors, significance levels for each effect could be interpreted directly. ANOVA results are summarized in Table 6, with full results listed in Appendix II.

Table 6. Summarized ANOVA results (significance and probabilities) for the effects of threshold methods and substrate correction on three accuracy measurements regarding fire mapping from the truth perspective.

| | | Accuracy Variables | | |
|---|---|---|---|---|
| Year | Factors | $A_{ET}/A_T$ | $A_{MI}/A_T$ | $A_{MO}/A_T$ |
| 1992 | | | | |
| | Threshold | *0.018* | *0.037* | *0.012* |
| | Correction | NS | NS | NS |
| | Threshold × Correction | NS | NS | NS |
| 1993 | | | | |
| | Threshold | *0.009* | *0.000* | NS |
| | Correction | NS | NS | NS |
| | Threshold × Correction | NS | NS | NS |
| 1995 | | | | |
| | Threshold | *0.000* | *0.000* | *0.014* |
| | Correction | NS | NS | NS |
| | Threshold × Correction | NS | NS | NS |

NS indicates non-significance at $\alpha = 0.05$, N = 63 (1992), N = 60 (1993), and N = 117 (1995).

Threshold factor is testing equality among three fixed effects.

Correction factor is testing equality among three fixed effects. Accuracy metrics comprising variables are ($A_{ET}$) area of total mapped fire event, ($A_T$) area of ground-truthing fire, ($A_{MI}$) area mapped within ground-truthing perimeters, and ($A_{MO}$) area mapped outside ground-truthing perimeters.

Scheffé's post hoc tests were conducted for each variable/year combination that showed significant differences for threshold methods in the ANOVA. These tests determined which of the three threshold methods differed significantly and whether any homogeneous subsets of threshold methods existed. Summarized results from the post hoc tests are in Table 7.

The results indicate that the double-threshold method ($X_3$) consistently expressed *event* area ($A_{ET}/A_T$) most accurately. Likewise, $X_3$ provided the best results for calculating areas mapped correctly within ground-truthing fire perimeters ($A_{MI}/A_T$). However, to reduce area mapped outside ground-truthing fire *events*, the strictest single-threshold method ($X_2$) was preferred.

Since effects of substrate corrections were not observed, the NDVI appeared relatively robust against substrate reflectance effects. Since NDVI robustness is not supported by the literature (e.g., Huete and Tucker 1991; Pereira 1999), potential faults with the general substrate-correction methods may exist. Stronger correction factors may be necessary to see pronounced effects.

The threshold/correction methods tested in this study may be detecting fires from previous seasons, thereby increasing values for the false detection variable and decreasing overall accuracy. Further studies referencing backward one or two fire seasons (e.g., Kasischke and French 1995) could test this hypothesis for Ontario. The event area consistently represents ground-truthing area more accurately than only the correctly mapped area (Figure 20).

Table 7. Scheffé's post hoc test results (significance and probabilities) for three accuracy measures among three threshold methods from the truth perspective.

| | | Accuracy Variables | | |
|---|---|---|---|---|
| Year | Comparison | $A_{ET}/A_T$ | $A_{MI}/A_T$ | $A_{MO}/A_T$ |
| 1992 | | | | |
| | $X_1$ and $X_2$ | NS | NS | NS |
| | $X_1$ and $X_3$ | *0.029* | *0.042* | *0.022* |
| | $X_2$ and $X_3$ | NS | NS | NS |
| 1993 | | | | |
| | $X_1$ and $X_2$ | NS | NS | |
| | $X_1$ and $X_3$ | NS | *0.000* | |
| | $X_2$ and $X_3$ | *0.013* | *0.000* | – |
| 1995 | | | | |
| | $X_1$ and $X_2$ | NS | NS | NS |
| | $X_1$ and $X_3$ | *0.005* | *0.000* | NS |
| | $X_2$ and $X_3$ | *0.002* | *0.000* | *0.027* |

Effects are ($X_1$, $X_2$) single-threshold methods, ($X_3$) double-threshold method, ($C_0$) no substrate correction, ($C_1$) slight substrate correction, and ($C_2$) high substrate correction. Accuracy metrics comprising variables are ($A_{ET}$) area of total mapped fire event, ($A_T$) area of ground-truthing fire, ($A_{MI}$) area mapped within ground-truthing perimeters, and ($A_{MO}$) area mapped outside ground-truthing perimeters. NS indicates non-significance at $\alpha = 0.05$, N = 63 (1992),

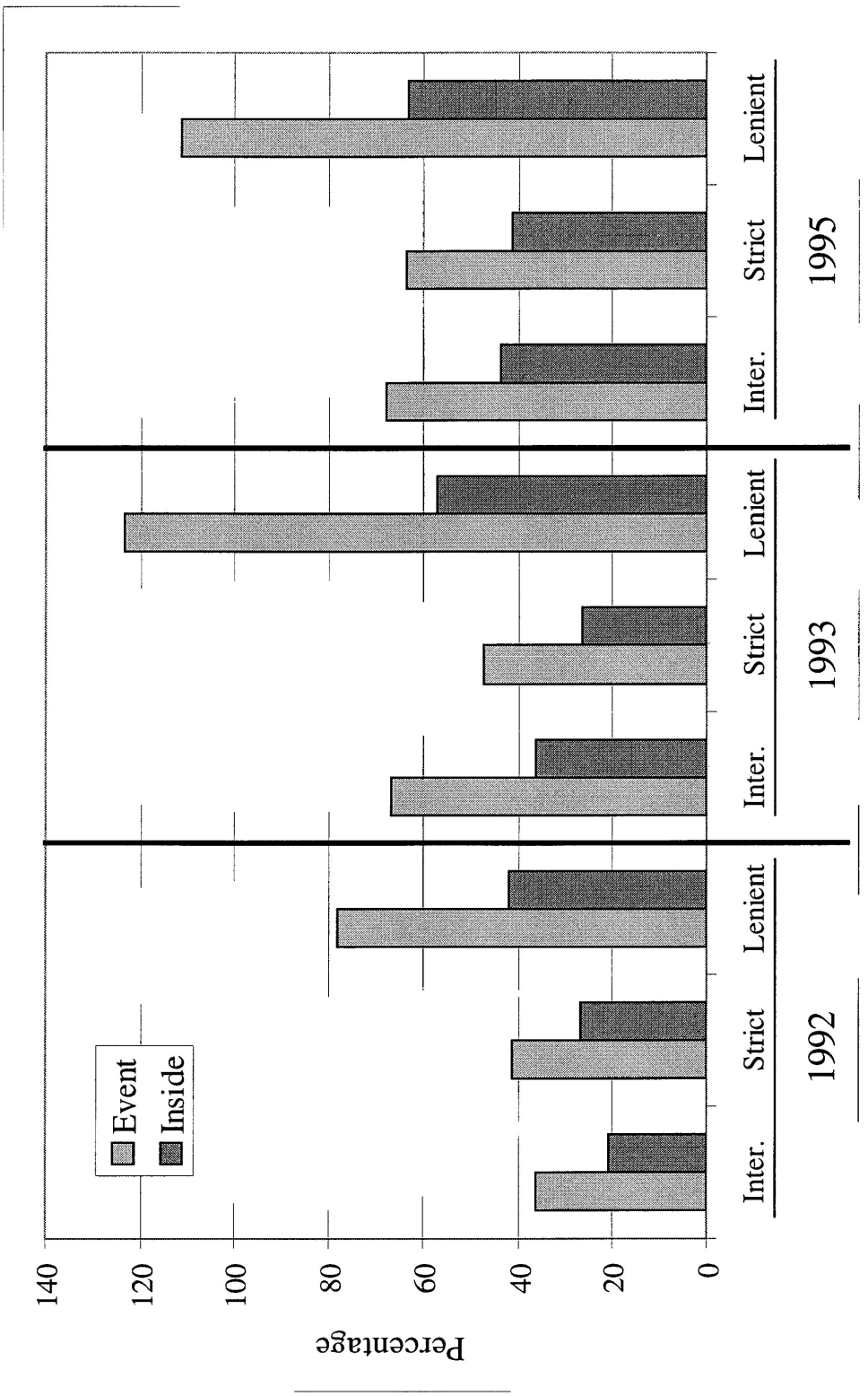


Figure 20. Comparing the accuracy of mapped fire-event area with area mapped inside ground-truthing perimeters. A percentage of 100 would indicate perfect areal correspondence between mapped and truthed areas.

### 4.2.2 Event Perspective

For the event perspective, the ANOVA tests (Table 8) found no significant differences ($p \geq 0.05$) among substrate correction effects or interaction effects between threshold methods and substrate corrections. Significant differences ($p < 0.05$) were found among threshold methods in all years for area unmapped within ground-truthing perimeters ($A_{UI}/A_T$), and for the 1992 area mapped outside variable ($A_{MO}/A_T$). Therefore, null hypotheses for substrate correction and threshold methods could not be rejected, except in the stated cases for $A_{UI}/A_T$ and $A_{MO}/A_T$. Since no significant interactions were observed among threshold methods and substrate correction factors, significance levels for each effect could be interpreted directly. ANOVA results are summarized in Table 8, with full results listed in Appendix II.

Scheffé's post hoc tests were conducted for each variable/year combination that showed significant differences for threshold methods in the ANOVA. These tests determined which threshold methods actually differed and whether any homogeneous subsets of threshold methods existed. Summarized results from the post hoc tests are listed in Table 9.

Table 8. Summarized ANOVA results (significance and probabilities) for the effects of threshold methods and substrate correction on three accuracy measurements regarding fire mapping from the event perspective.

| | | Accuracy Variables | | |
|---|---|---|---|---|
| Year | Factors | $A_{MI}/A_{ET}$ | $A_{MO}/A_{ET}$ | $A_{UI}/A_{ET}$ |
| 1992 | | | | |
| | Threshold | NS | *0.043* | *0.003* |
| | Correction | NS | NS | NS |
| | Threshold × Correction | NS | NS | NS |
| 1993 | | | | |
| | Threshold | NS | NS | *0.000* |
| | Correction | NS | NS | NS |
| | Threshold × Correction | NS | NS | NS |
| 1995 | | | | |
| | Threshold | NS | NS | *0.000* |
| | Correction | NS | NS | NS |
| | Threshold × Correction | NS | NS | NS |

NS indicates non-significance at $\alpha = 0.05$, N = 63 (1992), N = 60 (1993), and N = 117 (1995).

Threshold factor is testing equality among three fixed effects.

Correction factor is testing equality among three fixed effects. Accuracy metrics comprising variables are ($A_{MI}$) area mapped inside ground-truthing perimeters, ($A_{MO}$) area mapped outside ground-truthing perimeters, ($A_{UI}$) area unmapped within ground-truthing perimeters, and ($A_{ET}$) area of total mapped fire event.

Table 9. Scheffé's post hoc test results (significance and probabilities) for three accuracy measures among three threshold methods from the event perspective.

| Year | Comparison | Accuracy Variables $A_{MI}/A_{ET}$ | $A_{MO}/A_{ET}$ | $A_{UI}/A_{ET}$ |
|---|---|---|---|---|
| 1992 | | | | |
| | $X_1$ and $X_2$ | | NS | NS |
| | $X_1$ and $X_3$ | | NS | *0.005* |
| | $X_2$ and $X_3$ | | NS | *0.035* |
| 1993 | | | | |
| | $X_1$ and $X_2$ | | | *0.028* |
| | $X_1$ and $X_3$ | | | *0.022* |
| | $X_2$ and $X_3$ | | | *0.000* |
| 1995 | | | | |
| | $X_1$ and $X_2$ | | | NS |
| | $X_1$ and $X_3$ | | | *0.001* |
| | $X_2$ and $X_3$ | – | – | *0.000* |

Effects are ($X_1$, $X_2$) single-threshold methods, ($X_3$) double-threshold method, ($C_0$) no substrate correction, ($C_1$) slight substrate correction, and ($C_2$) high substrate correction. Accuracy metrics comprising variables are ($A_{MI}$) area mapped inside ground-truthing perimeters, ($A_{MO}$) area mapped outside ground-truthing perimeters, ($A_{UI}$) area unmapped within ground-truthed perimeters, and ($A_{ET}$) area of total mapped fire event. NS indicates non-significance at $\alpha = 0.05$, N = 63 (1992), N = 60 (1993), and N = 117 (1995).

Although the comparison of outside to event-area variable ($A_{MO}/A_{ET}$) in 1992 indicated significant differences with the ANOVA model, the post hoc tests indicated no significant differences among threshold methods. This discrepancy is attributed to the separation effect that post hoc tests introduce. Since the probability of inequality between the double and single threshold methods was almost significant, the added variance from the correction factors may have caused the ANOVA model to show significance. However, when separated, the threshold methods did not vary sufficiently among methods. Therefore, from the *event perspective*, only the variable that compared undetected area to the *event* area ($A_{UI}/A_{ET}$) indicated importance for selecting a suitable threshold method for fire mapping.

The double-threshold method ($X_3$) was found to differ significantly from both single-threshold methods ($X_1$ and $X_2$) for the $A_{UI}/A_{ET}$ variable. Areas unmapped inside truthing perimeters with the double-threshold method were the lowest; and omission was minimized due to the $X_3$ method incorporating fire areas identified by two different threshold methods.

### 4.2.3 Decision-Tree Analysis

Decision-tree analysis has been used to classify remotely sensed data (e.g., *Running et al.* 1995; Friedl and Brodley 1997). Each detected fire *event* in this study (n = 240) was classified using a decision-tree approach based on accuracy metric values (Figure 21). The decision tree provided a means for viewing accuracy visually, since numerical data were classified into one of six general *coincidence categories* occurring in the union

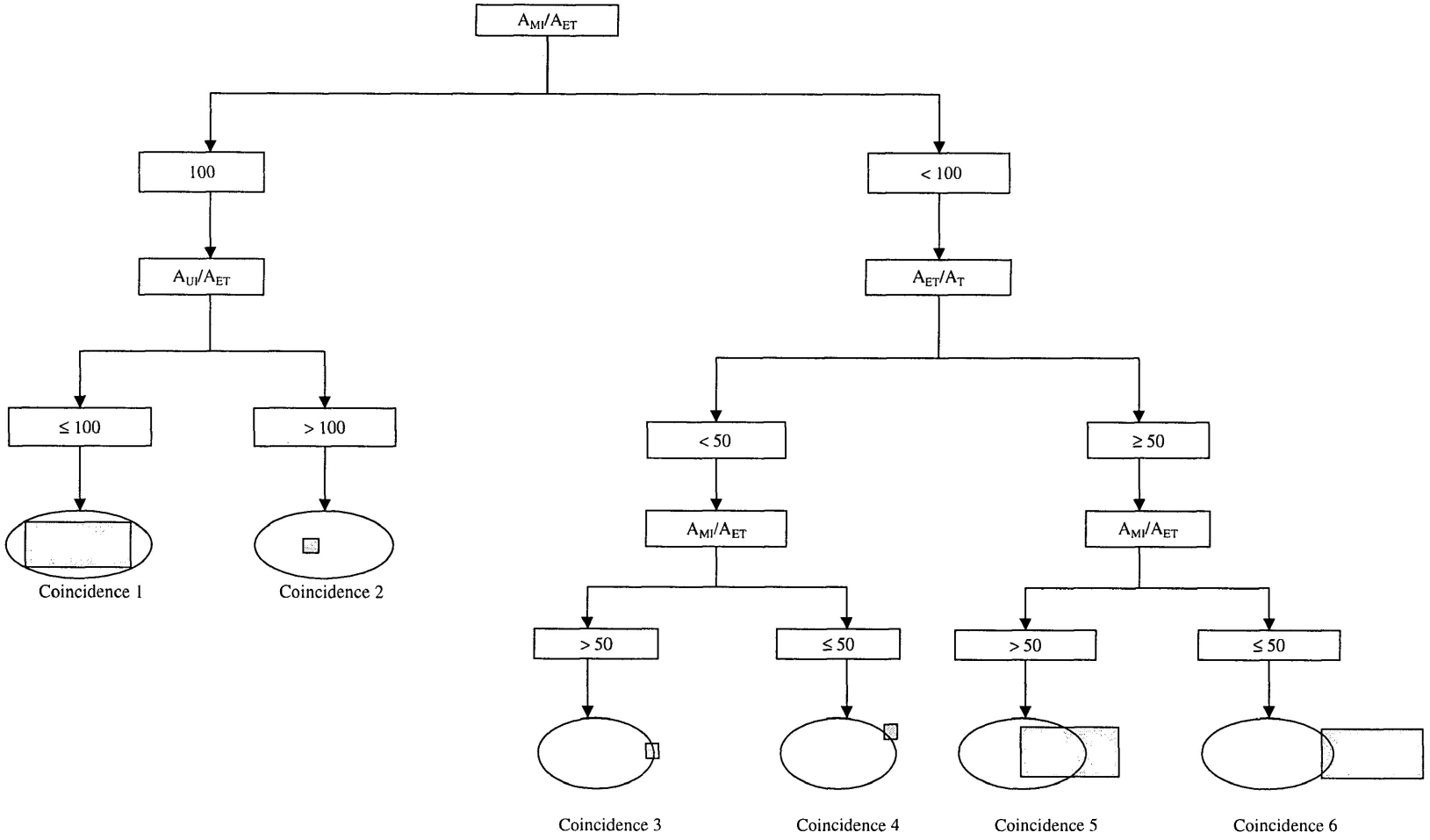


Figure 21. Decision tree resulting in six generalized coincidence categories in the union layer. Shaded rectangles represent mapped-fire events ($A_{ET}$), and ovals represent ground-truthing fire perimeters ($A_T$). Accuracy components making up variables are ($A_{MI}$) area mapped inside truthed perimeters, and ($A_{UI}$) area unmapped inside truthed perimeters. Conditions are actual variable values (percentages), with n = 240. All ratios are multiplied by 100.

layers. *Coincidence categories* were designated by generalizing overlap patterns of ground-truthing fire and detected-fire perimeters.

The results of the decision-tree analysis (Figure 22) indicate that although fires were not mapped with highest spatial and areal accuracy (*coincidence category* 1), mapped areas generally corresponded well with ground-truthing areas (*coincidence category* 5). Instances of mapping large areas outside ground-truthing fires (*coincidence category* 6) were low. Mapped areas contained fully by ground-truthing perimeters but having low areal correspondence (*coincidence category* 2) were also uncommon. Similarly, fires exhibiting poor areal correspondence with the majority of detected area outside ground-truthing perimeters (*coincidence category* 4) were rare. The high count for *coincidence category* 3 indicated that fires with low areal correspondence were generally well contained with the ground-truthing perimeters. A lower RMS error during geocorrection could result in improved accuracy, by spatially shifting cases within *coincidence categories* 3 and 4 to better correspond with ground-truthing fire perimeters.

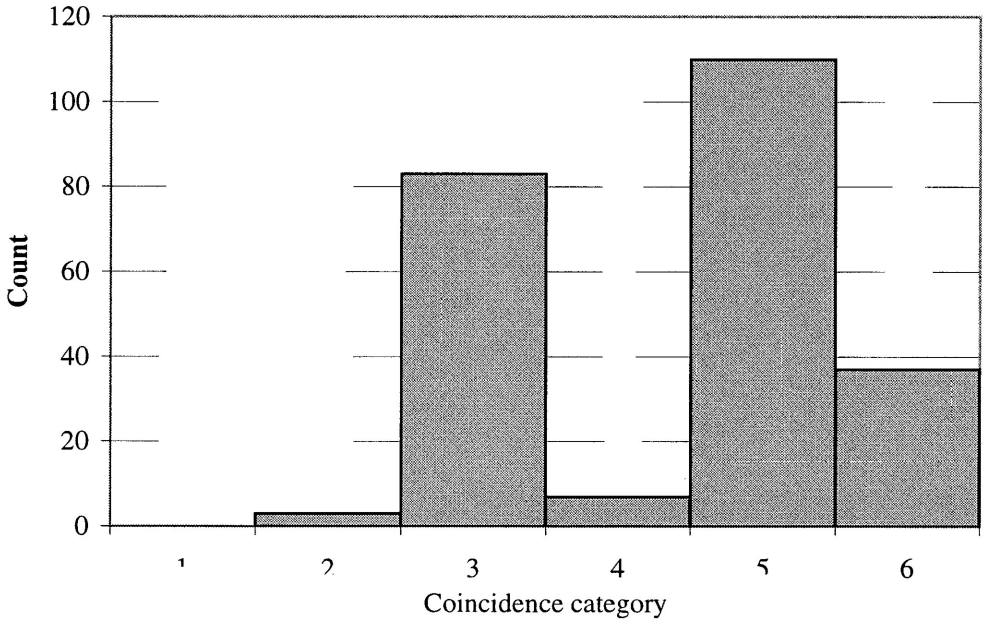


Figure 22. Decision-tree classification of detected fire events into coincidence categories (n = 240). Categories indicate levels of spatial coincidence among mapped-fire events and ground-truthing fire perimeters. Coincidence categories are (1) high areal and positional coincidence, (2) low areal but high positional coincidence, (3) low areal and reasonable positional coincidence, (4) low areal and low positional coincidence, (5) high areal but low positional coincidence, and (6) excessive mapped area and low positional coincidence.

### 4.2.4 Correlation Among Accuracy Metrics

To test the assumption that total mapped *event* area was associated with truthing-fire size, Pearson correlation coefficients were calculated (n = 240) for combinations of accuracy metrics used in this study (Table 10). Testing the correlation among all area metrics highlighted several significant ($p < 0.05$), positive relationships.

Both total *event* area ($A_{ET}$) and total ground-truthing area ($A_T$) were strongly correlated with the area mapped inside ground-truthing perimeters ($A_{MI}$). Total truthed-area ($A_T$) was also highly correlated with total *event* area ($A_{ET}$). Thus, it was concluded that as ground-truthing fire sizes increased, *event* area ($A_{ET}$) and area detected within ground-truthing perimeters ($A_{MI}$) also increased. Similar results were found by Kasischke *et al.* (1993) and Kasischke and French (1995).

Relationships among ground-truthing fire size ($A_T$) and area undetected ($A_{UI}$), or area mapped outside ground-truthing perimeters ($A_{MO}$) indicated moderate relationships. *Event* area ($A_{ET}$) was correlated highly with areas mapped inside ($A_{MI}$) and outside ($A_{MO}$) ground-truthing perimeters. Therefore, increasingly larger fires can be mapped with increasingly larger, contiguous areas ($A_{ET}$), both inside ($A_{MI}$) and outside ($A_{MO}$) ground-truthing perimeters.

Table 10. Pearson correlation coefficients and associated probabilities for accuracy metrics.

| | | $A_T$ | $A_{ET}$ | $A_{MI}$ | $A_{MO}$ | $A_{UI}$ |
|---|---|---|---|---|---|---|
| $A_T$ | **r** | | | | | |
| | *P* | | | | | |
| $A_{ET}$ | **r** | 0.863 | | | | |
| | *P* | *0.000* | | | | |
| $A_{MI}$ | **r** | 0.889 | 0.992 | | | |
| | *P* | *0.000* | *0.000* | | | |
| $A_{MO}$ | **r** | 0.629 | 0.875 | 0.805 | | |
| | *P* | *0.000* | *0.000* | *0.000* | | |
| $A_{UI}$ | **r** | 0.695 | 0.248 | 0.289 | 0.052 | |
| | *P* | *0.000* | *0.000* | *0.000* | *NS* | |

Cases (n = 240) were pooled from all 27 treatments. Correlation was tested among the metrics ($A_T$) total ground-truthing area, ($A_{UI}$) area undetected inside ground-truthing perimeters, ($A_{MI}$) area mapped inside ground-truthing perimeters, ($A_{MO}$) area mapped outside ground-truthing perimeters, and ($A_{ET}$) total fire event area. NS signifies non-significance at $\alpha = 0.05$.

# CHAPTER 5 – CONCLUSIONS

## SUMMARY OF FINDINGS

The accuracy assessment and decision-tree procedures developed in this study provided a simple and effective method for quantifying, visualizing, and partitioning accuracy for individual fire *events*. General trends regarding detected-area relationships with ground-truthing fire areas, among the different threshold methods, were generally comparable to those revealed in Alaska. However, the results of this study also indicate that existing methods for mapping post-fire disturbance patches with AVHRR/NDVI are not directly suited for use in northern Ontario.

The double-threshold method showed promise for mapping large wildfires, especially representing their general shapes. A strong correlation was found between the ability to detect and map fires with increasing fire size. However, the higher tendency of false-detection rate of the double-threshold method needs to be reduced, which is contradictory to results published by Kasischke and French (1993). Rigorous removal of translucent cloud contamination from AVHRR images could increase accuracy throughout the study, which is supported by Kasischke and French (1997).

No significant differences among substrate correction effects were found for any of the six accuracy variables (both perspectives) during the three fire seasons. In general, the double-threshold method consistently proved more effective than both of the single-threshold methods for accurately mapping areas within ground-truthing fire perimeters and for reducing omission. Consequently, the double-threshold method increased area

mapped outside ground-truthing fire perimeters and the area of false detection. This is explained by the inclusion of areas defined by the second threshold. Thus, to reduce omission and false detection, use of the strictest single-threshold method is recommended.

Ground-truthing fire sizes were found to be correlated with mapped event areas. Furthermore, these areas were highly correlated with correctly mapped area. Variability was high with respect to counting fire occurrences; thus, no technique was deemed satisfactory for consistently returning accurate counts of fire events.

The ability to partition accuracy into various components (mapped-area inside, mapped-area outside, etc.) from several perspectives allowed each fire mapping technique to be scrutinized at several levels. This technique provides deeper insight to the distribution of accuracy than do current techniques relying on predominantly fire-event area comparisons (i.e., $A_{ET}/A_T$) (e.g., Kasischke *et al.* 1993). Fire mapping techniques can be selected to emphasize specific accuracy components.

Accuracy results were not consistent among fire seasons, nor were they consistently within acceptable bounds for accurate fire mapping. Additionally, the proposed substrate corrections did not significantly improve the mapping accuracy of fire disturbance patches. Furthermore, only three years were studied; thus, limited replication may have contributed to inconsistencies among years. Increasing the years of study could help extract trends more representative of the study area.

## 5.2 FUTURE CONSIDERATIONS

Future research on fire detection and mapping in northern Ontario should focus on improving accuracy, specifically, reducing false detection. Adding a thermal channel for cloud extraction could improve fire detection and mapping algorithms (e.g., Flasse and Ceccato 1996). Fixed thresholds exhibit inherent hindrances due to variable climatic, topographic, radiometric, and spatial conditions of different study locations. Contextual thresholds (Fernández *et al.* 1997) may be more practical for studying dynamic landscapes, as could some human intervention to help isolate cloud-contaminated areas, thereby reducing the fully automated nature of these fire mapping algorithms. However, human intervention can be a source of random error, which can vary greatly among operators.

Development of binary and hierarchical classification schemes, using a variety of land-cover, soil, terrain, and vegetation data layers could provide unambiguous and context-sensitive methods for fire detection and mapping. Examples of these methods include decision-tree classification (Friedl and Brodley 1997) and regression tree analysis (Joel *et al.* 1994; Dobbertin and Biging 1997). The use of neural networks and fuzzy classifiers (Pal and Ghosh 1996) could provide opportunities for training decision-making during classification, to reduce susceptibility to local and temporal variations in data. Such classification procedures may involve the detection of core fire centres, followed by kernel growth algorithms to "fill" the remaining disturbance areas. Shorter

intervals between images may also be useful, especially for detecting disturbances in areas where rapid re-vegetation may occur.

The recently available, high-resolution Landsat 7 imagery, could be an economical option for smaller study areas requiring increased detail when mapping fires; however, for a 43-million hectare study area, an intermediate resolution between Landsat and AVHRR is preferred.

Some of the mentioned improvements may be met with the recently launched *Moderate Resolution Imaging Spectroradiometer (MODIS).* MODIS features a spatial resolution nearer to 0.5 km, onboard calibration, better atmospheric correction than AVHRR, and automated geo-location coding (Hu *et al.* 2000).

# LITERATURE CITED

Agbu, P.A. and M.E. James. 1994. NOAA/NASA Pathfinder AVHRR land data set user's manual. NASA, Goddard Space Flight Center, Goddard Distrubuted Active Archive Center, Greenbelt. MD. Various pagings.

Agriculture and Agri-Food Canada. 1996. Soil Landscapes of Canada, Version 2.2, National Soil Database.

Ashburn, P. 1979. The vegetative index number and crop identification. pp. 843-856 *in* Proceedings of the Technical Session, the LACIE Symposium, Huston, Texas, Oct. 3-26 1978. 1125 pp. (*Cited in* Jensen, 1996).

Beaubien, J. 1979. Forest type mapping from Landsat digital data. Photogrammetric Engineering & Remote Sensing **45**(8):1135-1144.

Bergeron, Y., S. Gauthier, C. Carcaillet, M. Flannigan, Y. Prairie and P.J.H. Richard. 1999. Variability in fire frequency and forest composition in Canada's southeastern boreal forest. pp. 74-81 *in* A challenge for sustainable forest management. The sustainable forest management network conference. Science and practice: Sustaining the boreal forest. Edmonton, Alberta, Canada, Feb. 14-17 1999. Various pagings.

Bryne, G.F., P.F. Crapper and K.K. Mayo. 1980. Monitoring land-cover change by principal component analysis of multitemporal Landsat data. Remote Sensing of Environment **10**:175-184.

Burke, R.A., R.G. Zepp, M.A. Tarr, W.L. Miller and B.J. Stocks. 1997. Effect of fire on soil-atmosphere exchange of methane and carbon dioxide in Canadian boreal forest sites. Journal of Geophysical Research **102**(D24):29289-29300.

Cahoon, D.R. Jr., B.J. Stocks, J.S. Levine, W.R. Cofer III and C.C. Chung. 1992. Evaluation of a technique for satellite-derived area estimation of forest fires. Journal of Geophysical Research **97**:3805-3814.

Cahoon, D.R. Jr., B.J. Stocks, J.S. Levine, W.R. Cofer III and J.M. Pierson. 1994. Satellite analysis of the severe 1987 forest fires in northern China and southeastern Siberia. Journal of Geophysical Research **99**(D9):18627-18638.

Cahoon, D.R. Jr., B.J. Stocks, J.S. Levine, W.R. Coffer III and J.A. Barber. 1996. Monitoring the 1992 forest fires in the boreal ecosystem using NOAA AVHRR satellite imagery. pp. 795-801 *in* Levine, J.S. (ed.) Biomass burning and global change, Volume 2. The MIT Press, London, England. 421 pp.

Chen, J.M. 1996. Evaluation of vegetation indices and a modified simple ratio for boreal applications. Canadian Journal of Remote Sensing **22**(3):229-242.

Collins, J.B. and C.E. Woodcock. 1996. An assessment of several linear change detection techniques for mapping forest mortality using multitemporal Landsat TM data. Remote Sensing of Environment **56**:66-77.

Condit, H.R. 1970. The spectral reflectance of American soils. Photogrammetric Engineering **36**:955-966.

Crown Forest Sustainability Act, Statutes of Ontario 1994, Chapter 25, Part I.

Curran, P.J. 1983. Estimating green LAI from multispectral aerial photography. Photogrammetric Engineering & Remote Sensing 55(5):601-610. (*Cited in* Jensen, 1996).

DeBano, L.F., D.G. Neary and P.F. Ffolliott. 1998. Fire's effects on ecosystems. John Wiley & Sons, Inc., New York. 333 pp.

Deering, D.W., J.W. Rouse, R.H. Haas and J.A. Schell. 1975. Measuring forage production of grazing units from Landsat MSS data. pp. 1169-1178 *in* Proceedings, 10th International Symposium on Remote Sensing of Environment, Volume 2, Ann Arbor, MI, Oct. 6-10 1975. Various pagings (*Cited in* Jensen, 1996).

Dobbertin, M. and G.S. Biging. 1998. Using the non-parametric classifier CART to model forest tree mortality. Forest Science **44**(4):507-516.

Dodge, A.G. and E.S. Bryant. 1976. Forest type mapping with satellite data. Journal of Forestry **74**:526-531.

Eastman, J.R. and M. Fulk. 1993. Long sequence time series evaluation using standardized principal components. Photogrammetric Engineering & Remote Sensing **59**(8):1307-1312.

Ecological Stratification Working Group. 1996. A national ecological framework for Canada. Canada: Minister of Supply and Services Canada. Canadian Soil Information System (CanSIS), Centre for Land and Biological Resources Research, Research branch, Agriculture and Agri-Food Canada.

Ehrlich, D., E.F. Lambin and J. Malingreau. 1997. Biomass burning and broad-scale land-cover changes in western Africa. Remote Sensing of Environment **61**:201-209.

Eidenshink, J.C. and J.L. Faundeen. 1994. The 1 km AVHRR global land data set: first stages in implementation. International Journal of Remote Sensing **15**(17):3443-3462.

Ens, D.K. 1987. Mapping of recent cutover/burnover areas using multi-date Landsat digital imagery. Saskatoon, Sask.: Saskatchewan Research Council. SRC Technical Report No. 197. Saskatchewan Technology Enhancement Program. 15 pp.

Environment Canada. 1998. National Climate Data Archive, Government of Canada, Canadian Meteorological Service.

Environmental Assessment Board. 1994. Reasons for decision and decision, Class environmental assessment by the Ministry of Natural Resources for timber management on Crown lands in Ontario, EA-87-02, Terms and Conditions. Ontario Ministry of Natural Resources.

Erdas, Inc. 1997. Erdas Imagine version 8.3.1, Build 59 (Windows NT), Erdas Inc.

ESRI, Inc. 1997. Arc/Info version 7.1.1 (UNIX), Environmental Systems Research Institute, Inc. Redlands, California, USA.

Eva, H. and E.F. Lambin. 1998. Remote sensing of biomass burning in tropical regions: Sampling issues and multisensor approach. Remote Sensing of Environment **64**:292-315.

Eve, M.D., W.G. Whitford and K.M. Havstadt. 1999. Applying satellite imagery to triage assessment of ecosystem health. Environmental Monitoring and Assessment **54**:205-227.

Farrar, J.L. 1995. Trees in Canada. Her Majesty the Queen in Right of Canada, Canada. 502 pp.

Fernández, A., P. Illera and J.L. Casanova. 1997. Automatic mapping of surfaces affected by forest fires in Spain using AVHRR NDVI composite image data. Remote Sensing of Environment **60**(2):153-162.

Filella, I. and J. Peñuelas. 1994. The red edge position and shape as indicators of plant chlorophyll content, biomass and hydric status. International Journal of Remote Sensing **15**(7):1459-1470.

Flasse, S.P. and P. Ceccato. 1996. A contextual algorithm for AVHRR fire detection. International Journal of Remote Sensing **17**(2):419-424.

French, N.H.F., L.L. Bourgeau-Chavez, Y. Yang and E.S. Kasischke. 1999. Initial observations of Radarsat imagery at fire-disturbed sites in interior Alaska. Remote Sensing of Environment **68**(1):89-94.

French, N.H.F., E.S. Kasischke, L.L. Bourgeau-Chavez and D. Berry. 1995. Mapping the location of wildfires in Alaskan boreal forests using AVHRR imagery. International Journal of Wildland Fire **5**(2):55-62.

French, N.H.F., E.S. Kasischke, R.D. Johnson, L.L. Bourgeau-Chavez, A.L. Frick and S. Ustin. 1996. Estimating fire-related carbon flux in Alaskan boreal forests using multisensor remote sensing data. pp. 808-826 *in* Levine, J.S. (ed.) Biomass burning and global change. Volume 2. The MIT Press, London, England. 421 pp.

Friedl, M.A. and C.E. Brodley. 1997. Decision tree classification of land cover from remotely sensed data. Remote Sensing of Environment **61**(3):399-409.

Gatlin, J.A., R.J. Sullivan and C.J. Tucker. 1983. Monitoring global vegetation using NOAA-7 AVHRR data. 1983. *in* International Geoscience and Remote Sensing Symposium (IGARSS '83). San Francisco, California, Aug. 31–Sept. 2 1983. Various pagings.

Gillis, M.D. and D.G. Leckie. 1993. Forest inventory mapping procedures across Canada. Petawawa National Forestry Institute, Forestry Canada, Chalk River, Ontario. Information Report PI-X-114. 79 pp.

Gillis, M.D. and D.G. Leckie. 1996. Forest inventory update in Canada. The Forestry Chronicle **72**(2):138-156.

Gonzalez-Alonso, F., J.L. Casanova, A. Calle, J.M. Cuevas and P. Illera. 1996. Application of the NOAA-AVHRR images to the study of the large forest fires in Spain in the summer of 1994. International Journal of Remote Sensing **17**(6):1089-1091.

Goward, S.N., C.J. Tucker and D.G. Dye. 1985. North American vegetation patterns observed with the NOAA-7 advanced very high resolution radiometer. Vegetatio **64**:3-14.

Guyette, R.P. and D.C. Dey 1995. A dendrochronological fire history of Opeongo lookout in Algonquin Park. Ontario Ministry of Natural Resources, Ontario Forest Research Institute, Sault Ste. Marie, Ontario. Forest research report No. 134. 4 pp.

Heinselman, M.L. 1981. Fire intensity and frequency as factors in the distribution and structure of northern ecosystems. pp. 7-57. *in* Mooney, H.A, T.M. Bonnicksen, N.L. Christensen, J.E. Lotan and W.A. Reiners (ed.) Proceedings of the conference - Fire regimes and ecosystem properties. General Technical Report WO-26. Honolulu, Hawaii, Dec. 11-15 1981. 594 pp.

Holben, B.N. 1986. Characteristics of maximum-value composite images from temporal AVHRR data. International Journal of Remote Sensing **7**(11):1417-1434.

Hopkins, P.F., A.L. Maclean and T.M. Lillesand. 1988. Assessment of thematic mapper imagery for forestry applications under Lake States conditions. Photogrammetric Engineering & Remote Sensing **54**(1):61-68.

Horler, D.N.H., M. Dockray and J. Barber. 1983. The red edge of plant leaf reflectance. International Journal of Remote Sensing **4**(2):273-288.

Hu, B., W. Lucht, A.H. Strahler, C.B. Schaaf and M. Smith. 2000. Surface albedos and angle-corrected NDVI from AVHRR observations of South America. Remote Sensing of Environment **71**:119-132.

Huete, A.R. 1988. A soil-adjusted vegetation index (SAVI). Remote Sensing of Environment **25**:295-309.

Huete, A.R. and C.J. Tucker. 1991. Investigation of soil influences in AVHRR red and near-infrared vegetation index imagery. International Journal of Remote Sensing **12**(6):1223-1242.

Iverson, L.R., R.L. Graham and E.A. Cook. 1989. Applications of satellite remote sensing to forested ecosystems. Landscape Ecology **3**(2):131-143.

Jakubauskas, M.E., K.P. Lulla and P.W. Mausel. 1990. Assessment of vegetation change in a fire-altered forest landscape. Photogrammetric Engineering & Remote Sensing **56**(3):371-377.

Johnson, E.A. 1992. Fire and vegetation dynamics: Studies from the North American boreal forest. Cambridge University Press, Great Britain. 129 pp.

Justice, C.O., J.D. Kendall, P.R. Dowty and R.J. Scholes. 1996. Satellite remote sensing of fires during the SAFARI campaign using NOAA advanced very high resolution radiometer data. Journal of Geophysical Research **101**(D19):23851-23863.

Kasischke, E.S. and N.H.F. French. 1995. Locating and estimating the areal extent of wildfires in Alaskan boreal forests using multiple-season AVHRR NDVI composite data. Remote Sensing of Environment **51** (2):263-275.

Kasischke, E.S. and N.H.F. French. 1997. Constraints on using AVHRR composite imagery to study patterns of vegetation cover in boreal forests. International Journal of Remote Sensing **18**(11):2403-2426.

Kasischke, E.S., N.H.F. French, P. Harrell, N.L. Christensen Jr., S.L. Ustin and D. Barry. 1993. Monitoring of wildfires in boreal forests using large area AVHRR NDVI composite image data. Remote Sensing of Environment **45**(1):61-71.

Kauth, R.J. and G.S. Thomas. 1976. The tasseled cap—A graphic description of the spectral-temporal development of agricultural crops as seen by Landsat. pp. 41-51. *in* Proceedings, Symposium on machine processing of remotely sensed data, Purdue University, Laboratory for Applications of Remote Sensing, West Lafayette, IN, Jun. 29-Jul. 1 1976. 336 pp.

Kidwell, K.B. 1991. NOAA polar orbiter data users guide (TIROS-N, NOAA-6, NOAA-7, NOAA-8, NOAA-9, NOAA-10, NOAA-11, and NOAA-12). U.S. Department of Commerce, National Oceanic and Atmospheric Administration Washington, National Environmental Satellite, Data, and Information Service, Washington. Various pagings.

King, D.J. 1995. Airborne multispectral digital camera and video sensors: a critical review of system designs and applications. Canadian Journal of Remote Sensing, Special Issue on Aerial Optical Remote Sensing **21**(3):245-273.

Landry, R., F.J. Ahern, and R. O'Neil. 1995. Forest burn visibility on C-HH radar images. Canadian Journal of Remote Sensing **21**(2):204-206.

Larsen, C.P.S. and G.M. MacDonald. 1998. An 840-year record of fire and vegetation in a boreal white spruce forest. Ecology **79**(1):106-118.

Larsson, H. 1993. Linear regressions for canopy cover estimation in Acacia woodlands using Landsat-TM, -MSS and SPOT HRV XS data. International Journal of Remote Sensing **14**(11):2129-2136.

Leblanc, S.G., J.M. Chen and J. Cihlar. 1997. NDVI directionality in boreal forests: A model interpretation of measurements. Canadian Journal of Remote Sensing **23**(4):369-380.

Levine, J.S., D.R. Cahoon Jr., J.A. Costulis, R.H. Couch, R.E. Davis, P.A. Garn, A. Jalink Jr., J.A. McAdoo, D.M. Robinson, W.A. Roettker, W.A. Sasamoto, R.T. Sherrill and K.D. Smith. 1996. FireSat and the global monitoring of biomass burning. pp. 107-129 *in* Levine, J.S. (ed.) Biomass burning and global change, Volume 1, The MIT Press, London, England. 632 pp.

Li, Z., J. Cihlar, L. Moreau, F. Huang and B. Lee. 1997. Monitoring fire activities in the boreal ecosystem. Journal of Geophysical Research **102**(D24):29611-29624.

Li, Y., T.H. Demetriades-Shah, E.T. Kanemasu, J.K. Shultis and M.B. Kirkham. 1993. Use of second derivatives of canopy reflectance for monitoring prairie vegetation over different soil backgrounds. Remote Sensing of Environment **44**(1):81-87.

Jensen, J.R. 1996. Introductory digital image processing a remote sensing perspective. Second Edition. Prentice-Hall, Inc., Upper Saddle River, New Jersey. 316 pp.

Lillesand, T.M. and R.W. Kiefer. 1994. Remote sensing and image interpretation: Third edition. John Wiley & Sons, Inc, New York. 750 pp.

López, S., F. González, R. Llop and J.M. Cuevas. 1991. An evaluation of the utility of NOAA AVHRR images for monitoring forest fire risk in Spain. International Journal of Remote Sensing **12**(9):1841-1851.

Loveland, T.R. and A.S. Belward. 1997. The IGBP-DIS global 1 km land cover data set, DISCover: first results. International Journal of Remote Sensing **18**(15):3289-3295.

Lunetta, R.S. and C.D. Elvidge. 1998. Remote sensing change detection, environmental monitoring methods and applications. Ann Arbor Press, USA. 318 pp.

Lynham, T. J. and B.J. Stocks. 1991. The natural fire regime of an unprotected section of the boreal forest in Canada. pp. 99-109 *in* Proceedings: 17th Tall timbers fire ecology conference. Tallahassee, Florida, May 18-21 1989. 435 pp.

MacDonald, G.M., C.P.S. Larsen, J.M. Szeicz and K.A. Moser. 1991. The reconstruction of boreal forest fire history from lake sediments: A comparison of charcoal, pollen, sedimentological, and geochemical indices. Quaternary Science Reviews **10**(1):53-71.

Madill, R.J. and A.H. Aldred. 1977. Forest resources mapping in Canada. The Canadian Surveyor **31**(1):9-20.

Major, D.J., F. Baret and G. Guyot. 1990. A ratio vegetation index adjusted for soil brightness. International Journal of Remote Sensing **11**(5):727-740.

Marsh, S.E., J.L. Walsh, C.T. Lee, L.R. Beck and C.F. Hutchinson. 1992. Comparison of multi-temporal NOAA-AVHRR and SPOR-XS satellite data for mapping land-cover dynamics in the west African Sahel. International Journal of Remote Sensing **13**(16):2997-3016.

Martell, D.L. and D. Boychuk. 1997. Levels of fire protection for sustainable forestry in Ontario: A discussion paper. Natural Resources Canada, Canadian Forest Service, Great Lakes Forestry Centre, Sault Ste. Marie, Ontario. NODA/NFP Technical Report TR-43. 34 pp.

Martín, M.P. and E. Chuvieco. 1995. Mapping and evaluation of burned land from multitemporal analysis of AVHRR NDVI images. EARSeL Advances in Remote Sensing **4**(3):7-13.

Matson, M., G. Stephens and J. Robinson. 1987. Fire detection using data from the NOAA-N satellites. International Journal of Remote Sensing **8**(7):961-970.

Medler, M.J. and S.R. Yool. 1997. Improving Thematic Mapper based classification of wildfire induced vegetation mortality. Geocarto International **12**(1):49-58.

Michaelsen, J., D.S. Schimel, M.A. Friedl, F.W. Davis and R.C. Dubayah. 1994. Regression tree analysis of satellite and terrain data to guide vegetation sampling and surveys. Journal of Vegetation Science **5**:673-686.

Milne, A.K. 1988. Change direction analysis using Landsat imagery: a review of methodology. Proceedings of IGARSS '88 Symposium. Edinburgh, Scotland, Sept. 3-16 1988. 1858 pp.

Misra, P.N. and S.G. Wheeler. 1977. Landsat data from agricultural sites–crop signature analysis. *in* Proceedings, 11th International Symposium on Remote Sensing of the Environment, Ann Arbor, MI, Apr. 25-29 1977. 1668 pp. (*Cited in* Jensen, 1996).

Nemani, R. and S. Running. 1997. Land cover characterization using multitemporal red, near-IR, and thermal-IR data from NOAA/AVHRR. Ecological Applications **7**(1):79-90.

Pal, S.K. and A. Ghosh. 1996. Review, Neuro-fuzzy computing for image processing and pattern recognition. International Journal of Systems Science **27**(12):1179-1193.

Patterson, M.W. and S.R. Yool. 1998. Mapping fire-induced vegetation mortality using Landsat Thematic Mapper data: A comparison of linear transformation techniques. Remote Sensing of Environment **65**:132-142.

Pereira, J.M.C. 1999. A comparative evaluation of NOAA/AVHRR vegetation indexes for burned surface detection and mapping. IEEE Transactions on Geoscience and Remote Sensing **37**(1):217-226.

Pereira, M.C. and A.W. Setzer. 1993a. Spectral characteristics of deforestation fires in NOAA/AVHRR images. International Journal of Remote Sensing **14**(3):583-597.

Pereira, M.C. and A.W. Setzer. 1993b. Spectral characteristics of fire scars in Landsat-5 TM images of Amazonia. International Journal of Remote Sensing **14**(11):2061-2078.

Perera, A.H., D.J.B. Baldwin, F. Schnekenburger, J.E. Osborne and R.E. Bae. 1998. Forest fires in Ontario: A spatio-temporal perspective. Ontario Ministry of Natural Resources, Ontario Forest Research Institute, Sault Ste. Marie, Ontario. Forest Research Report No. 147. 22 pp.

Perry, C.R. and L.F. Lautenschlager. 1984. Functional equivalence of spectral vegetation indices. Remote Sensing of Environment **14**:169-182.

Pozo, D., F.J. Olmo and L. Alados-Arboledas. 1997. Fire detection and growth monitoring using a multitemporal technique on AVHRR mid-infrared and thermal channels. Remote Sensing of Environment **60**(2):111-120.

Price, J.C. 1987. Calibration of satellite radiometers and the comparison of vegetation indices. Remote Sensing of Environment **21**:15-27.

Rao, C.R.N. 1987. Pre-launch calibration of channels 1 and 2 of the Advanced Very High Resolution Radiometer. U.S. Department of Commerce, National Oceanic and Atmospheric Administration, Satellite Research Laboratory, National Environmental Satellite, Data, and Information Service, Washington, D.C. NOAA Technical Report NESDIS 36. 63 pp.

Rauste, Y., E. Herland, H. Frelander, K. Soini, T. Kuoremäki and A. Ruokari. 1997. Satellite-based forest fire detection for fire control in boreal forests. International Journal of Remote Sensing **18** (12):2641-2656.

Razafimpanilo, H., R. Frouin, S.F. Iacobellis and C.J. Somerville. 1995. Methodology for estimating burned area from AVHRR reflectance data. Remote Sensing of Environment **54**(3):273-289.

Richards, J.A. and A.K. Milne. 1983. Mapping fire burns and vegetation regeneration using principal components analysis. pp. 5.1-5.6 *in* International Geoscience and Remote Sensing Symposium (IGARSS '83), San Francisco, California, Aug. 31-Sep. 2 1983. Various pagings.

Richardson, A.J. and C.L. Wiegand. 1977. Distinguishing vegetation from soil background information. Photogrammetric Engineering & Remote Sensing **43**(12):1541-1552.

Robinson, J.M. 1991. Fire from space: Global fire evaluation using infrared remote sensing. International Journal of Remote Sensing **12**(1):3-24.

Roderick, M., R. Smith and S. Cridland. 1996. The precision of the NDVI derived from AVHRR observations. Remote Sensing of Environment **56**:57-65.

Roller, N.E.G. and J.E. Colwell. 1986. Coarse-resolution satellite data for ecological surveys. BioScience **36**(7):468-475.

Rouse, J.W., R.H. Haas, J.A. Schell and D.W. Deering. 1973. Monitoring vegetation systems in the great plains with ERTS. pp. 48-62 *in* Proceedings, 3rd ERTS Symposium, Goddard Space Flight Center, Greenbelt, MD, Washington, DC, Dec. 10-14 1973. 117 pp.

Running, S.W., T.R. Loveland, L.L. Pierce, R.R. Nemani and E.R. Hunt Jr. 1995. A remote sensing based vegetation classification logic for global land cover analysis. Remote Sensing of Environment **51**:39-48.

SPSS, Inc. 1997. SPSS for windows, release 8.0.0 (Windows NT), SPSS Inc. Chicago, Illinois, USA.

Steyaert, T., F.G. Hall and T.R. Loveland. 1997. Land cover mapping, fire regeneration, and scaling studies in the Canadian boreal forest with 1 km AVHRR and Landsat TM data. Journal of Geophysical Research **102**(D24):29581-29598.

Stoner, E.R. and M.F. Baumgardner. 1981. Characteristic variations in reflectance of surface soils. Soil Science Society of America Journal **45**:1161-1165.

Teuber, K.B. 1990. Use of AVHRR imagery for large-scale forest inventories. Forest Ecology and Management **33/34**:621-631.

Townshend, J.R.G. and C.O. Justice. 1986. Analysis of the dynamics of African vegetation using the normalized difference vegetation index. International Journal of Remote Sensing **7**(11):1435-1445.

Townshend, J.R.G., C.O. Justice, D. Skole, J.P. Malingreau, J. Cihlar, P. Teillet, F. Sadowski and S. Ruttenberg. 1994. The 1 km resolution global data set: needs of the International Geosphere Biosphere Programme. International Journal of Remote Sensing **15**(17):3417-3441.

Tucker, C.J. 1979. Red and photographic infrared linear combinations for monitoring vegetation. Remote Sensing of Environment **8**:12-150.

Tucker, C.J., R.G. Townshend and T.E. Goff. 1985. African land-cover classification using satellite data. Science **227**(4685):369-375.

Viedma, O., J. Meliá, D. Segarra and J. García-Haro. 1997. Modeling rates of ecosystem recovery after fires by using Landsat TM data. Remote Sensing of Environment **61**:383-398.

Viovy, N., O. Arino and A.S. Belward. 1992. The Best Index Slope Extraction (BISE): A method for reducing noise in NDVI time-series. International Journal of Remote Sensing **13**(8):1585-1590.

Whelan, R.J. 1995. The ecology of fire. Cambridge University Press, New York. 346 pp.

White, J.D., K.C. Ryan, C.C. Key and S.W. Running. 1996. Remote sensing of forest fire severity and vegetation recovery. International Journal of Wildland Fire **6**(3):125-136.

Williams, A.M. 1953. Determining burned area by aerial mapping. Journal of Forestry **51**(11):825-826.

Woodcock, C.E., J.B. Collins, S. Gopal, V.D. Jakabhazy, X. Li, S. Macomber, S. Ryherd, V.J. Horward, J. Levitan, Y. Wu and R. Warbington. 1994. Mapping forest vegetation using Landsat TM imagery and a canopy reflectance model. Remote Sensing of Environment **50**(3):240-254.

Zepp, R.G., W.L. Miller, M.A. Tarr, R.A. Burke and B.J. Stocks. 1997. Soil-atmosphere fluxes of carbon monoxide during early stages of postfire succession in upland Canadian boreal forests. Journal of Geophysical Research **102**(D24):29301-29311.

# APPENDIX I

## Common Vegetation Indices

Common vegetation indices.

| Acronym | Name | Platform | Detects | Reference | Formula |
|---|---|---|---|---|---|
| NDVI | Normalized Difference Vegetation Index | TM | Vegetation | Marsh *et al.* (1992) | $NDVI = \frac{(TM4 - TM3)}{(TM4 + TM3)}$ |
| | | SPOT HRV | Vegetation | Larsson (1993) | $NDVI = \frac{(XS3 - XS2)}{(XS3 + XS2)}$ |
| | | AVHRR | Vegetation | Eastman and Fulk (1993) | $NDVI = \frac{(NIR - R)}{(NIR + R)}$ |
| | | MSS | Vegetation | Rouse *et al.* (1973) | * $NDVI = \frac{(MSS6 - MSS5)}{(MSS6 + MSS5)}$ |
| | | MSS | Vegetation | | ** $NDVI = \frac{(MSS7 - MSS5)}{(MSS7 + MSS5)}$ |
| TVI | Transformed Vegetation Index | MSS | Vegetation | Deering *et al.* (1975)† | $TVI = \sqrt{NDVI^{*} + 0.5}$ |
| | | MSS | Vegetation | | $TVI = \sqrt{NDVI^{**} + 0.5}$ |
| | | MSS | Vegetation | Perry and Lautenschlager (1984) | $TVI = \frac{NDVI^{*} + 0.5}{\lvert NDVI^{*} + 0.5 \rvert} \times \sqrt{\lvert NDVI^{*} \rvert}$ |

† As cited in Jensen (1996).

Common vegetation indices (continued).

| Acronym | Name | Platform | Detects | Reference | Formula |
|---|---|---|---|---|---|
| AVI | Ashburn Vegetation Index | MSS | Vegetation | Ashburn (1978) | $AVI = 2.0MSS7 - MSS5$ |
| PVI | Perpendicular Vegetation Index | MSS | Vegetation/soil | Richardson and Wiegand (1977)<br>Curran (1983)† | $PVI = \left[\begin{matrix}(-2.507 - 0.457MSS5 + 0.498MSS6)^2 \\ +(2.734 + 0.498MSS5 - 0.543MSS6)^2\end{matrix}\right]^{\frac{1}{2}}$ |
| | | MSS | Vegetation/soil | | $PVI = \left[\begin{matrix}(0.355MSS7 - 0.149MSS5)^2 \\ +(0.355MSS5 - 0.852MSS7)^2\end{matrix}\right]^{\frac{1}{2}}$ |
| | | MSS | Vegetation/soil | Perry and Lautenschlager (1984) | $PVI = \frac{1.091MSS6 - MSS5 - 5.49}{\sqrt{1.091^2 + 1}}$ |
| | | MSS | Vegetation/soil | | $PVI = \frac{2.4MSS7 - MSS5 - 0.01}{\sqrt{2.4^2 + 1}}$ |
| SAVI | Soil Adjusted Vegetation Index | Various | Vegetation/soil | Huete (1988) | $SAVI = \frac{\rho_{nir} + L_1}{\rho_{red} + L_2}$ |
| | | Various | Vegetation/soil | Major *et al.* (1990) | $SAVI = \frac{\rho_{nir}}{\rho_{red+\Phi}}$ |
| TCA | Tasseled Cap Analysis | MSS/TM | Greenness/soil | Kauth and Thomas (1976) | |
| PCA | Principle Component Analysis | MSS | Vegetation | Misra and Wheeler (1977)† | |

† As cited in Jensen (1996).

# APPENDIX II

## ANOVA Tables

Results of ANOVA on measures of spatial coincidence during 1992.

| Variable | Factors | Type III SS | df | MS | *F* | *P* |
|---|---|---|---|---|---|---|
| $A_{ET}/A_T$ | Model | 0.209 | 9 | 0.023 | 31.303 | 0.000 |
| | Threshold | 0.006 | 2 | 0.003 | 4.307 | **0.018** |
| | Correction | 0.000 | 2 | 0.000 | 0.001 | 0.999 |
| | Threshold × Correction | 0.000 | 4 | 0.000 | 0.005 | 1.000 |
| | Error | 0.040 | 54 | 0.001 | | |
| | Total | 0.249 | 63 | | | |
| $A_{MI}/A_T$ | Model | 0.119 | 9 | 0.013 | 33.602 | 0.000 |
| | Threshold | 0.003 | 2 | 0.001 | 3.505 | **0.037** |
| | Correction | 0.000 | 2 | 0.000 | 0.000 | 1.000 |
| | Threshold × Correction | 0.000 | 4 | 0.000 | 0.008 | 1.000 |
| | Error | 0.021 | 54 | 0.000 | | |
| | Total | 0.141 | 63 | | | |
| $A_{MO}/A_T$ | Model | 0.082 | 9 | 0.009 | 18.238 | 0.000 |
| | Threshold | 0.005 | 2 | 0.002 | 4.841 | **0.012** |
| | Correction | 0.000 | 2 | 0.000 | 0.010 | 0.990 |
| | Threshold × Correction | 0.000 | 4 | 0.000 | 0.003 | 1.000 |
| | Error | 0.027 | 54 | 0.000 | | |
| | Total | 0.109 | 63 | | | |
| $A_{MI}/A_{ET}$ | Model | 0.233 | 9 | 0.026 | 89.274 | 0.000 |
| | Threshold | 0.001 | 2 | 0.000 | 1.575 | 0.216 |
| | Correction | 0.000 | 2 | 0.000 | 0.005 | 0.995 |
| | Threshold × Correction | 0.000 | 4 | 0.000 | 0.004 | 1.000 |
| | Error | 0.016 | 54 | 0.000 | | |
| | Total | 0.249 | 63 | | | |
| $A_{MO}/A_{ET}$ | Model | 0.130 | 9 | 0.014 | 49.781 | 0.000 |
| | Threshold | 0.002 | 2 | 0.001 | 3.342 | **0.043** |
| | Correction | 0.000 | 2 | 0.000 | 0.054 | 0.947 |
| | Threshold × Correction | 0.000 | 4 | 0.000 | 0.006 | 1.000 |
| | Error | 0.016 | 54 | 0.000 | | |
| | Total | 0.145 | 63 | | | |
| $A_{UI}/A_{ET}$ | Model | 1.095 | 9 | 0.122 | 16.507 | 0.000 |
| | Threshold | 0.097 | 2 | 0.049 | 6.602 | **0.003** |
| | Correction | 0.001 | 2 | 0.000 | 0.037 | 0.964 |
| | Threshold × Correction | 0.000 | 4 | 0.000 | 0.014 | 1.000 |
| | Error | 0.398 | 54 | 0.007 | | |
| | Total | 1.493 | 63 | | | |

Metrics used in accuracy variables are total area of mapped fire event ($A_{ET}$), total area of ground-truthing fire ($A_T$), area mapped inside ground-truthing perimeters ($A_{MI}$), area mapped outside ground-truthing perimeters ($A_{MO}$), and area undetected inside ground-ruthing perimeters ($A_{UI}$). All tests were conducted with n = 240 and a = 0.05.

Results of ANOVA on measures of spatial coincidence during 1993.

| Variable | Factors | Type III SS | df | MS | *F* | *P* |
|---|---|---|---|---|---|---|
| $A_{ET}/A_T$ | Model | 0.304 | 9 | 0.034 | 29.672 | 0.000 |
| | Threshold | 0.012 | 2 | 0.006 | 5.129 | **0.009** |
| | Correction | 0.000 | 2 | 0.000 | 0.002 | 0.998 |
| | Threshold × Correction | 0.000 | 4 | 0.000 | 0.000 | 1.000 |
| | Error | 0.058 | 51 | 0.001 | | |
| | Total | 0.362 | 60 | | | |
| $A_{MI}/A_T$ | Model | 0.153 | 9 | 0.017 | 207.320 | 0.000 |
| | Threshold | 0.004 | 2 | 0.002 | 22.887 | **0.000** |
| | Correction | 0.000 | 2 | 0.000 | 0.077 | 0.926 |
| | Threshold × Correction | 0.000 | 4 | 0.000 | 0.003 | 1.000 |
| | Error | 0.004 | 51 | 0.000 | | |
| | Total | 0.157 | 60 | | | |
| $A_{MO}/A_T$ | Model | 0.128 | 9 | 0.014 | 9.766 | 0.000 |
| | Threshold | 0.008 | 2 | 0.004 | 2.774 | 0.072 |
| | Correction | 0.000 | 2 | 0.000 | 0.000 | 1.000 |
| | Threshold × Correction | 0.000 | 4 | 0.000 | 0.000 | 1.000 |
| | Error | 0.074 | 51 | 0.001 | | |
| | Total | 0.202 | 60 | | | |
| $A_{MI}/A_{ET}$ | Model | 0.231 | 9 | 0.026 | 153.876 | 0.000 |
| | Threshold | 0.000 | 2 | 0.000 | 1.124 | 0.333 |
| | Correction | 0.000 | 2 | 0.000 | 0.007 | 0.993 |
| | Threshold × Correction | 0.000 | 4 | 0.000 | 0.001 | 1.000 |
| | Error | 0.009 | 51 | 0.000 | | |
| | Total | 0.240 | 60 | | | |
| $A_{MO}/A_{ET}$ | Model | 0.122 | 9 | 0.014 | 68.459 | 0.000 |
| | Threshold | 0.001 | 2 | 0.000 | 2.185 | 0.123 |
| | Correction | 0.000 | 2 | 0.000 | 0.002 | 0.998 |
| | Threshold × Correction | 0.000 | 4 | 0.000 | 0.000 | 1.000 |
| | Error | 0.010 | 51 | 0.000 | | |
| | Total | 0.133 | 60 | | | |
| $A_{UI}/A_{ET}$ | Model | 0.487 | 9 | 0.054 | 35.381 | 0.000 |
| | Threshold | 0.047 | 2 | 0.023 | 15.315 | **0.000** |
| | Correction | 0.000 | 2 | 0.000 | 0.003 | 0.997 |
| | Threshold × Correction | 0.000 | 4 | 0.000 | 0.000 | 1.000 |
| | Error | 0.078 | 51 | 0.002 | | |
| | Total | 0.565 | 60 | | | |

Metrics used in accuracy variables are total area of mapped fire event ($A_{ET}$), total area of ground-truthing fire ($A_T$), area mapped inside ground-truthing perimeters ($A_{MI}$), area mapped outside ground-truthing perimeters ($A_{MO}$), and area undetected inside ground-ruthing perimeters ($A_{UI}$). All tests were conducted with n = 240 and a = 0.05.

Results of ANOVA on measures of spatial coincidence during 1995.

| Variable | Factors | Type III SS | df | MS | *F* | *P* |
|---|---|---|---|---|---|---|
| $A_{ET}/A_T$ | Model | 0.593 | 9 | 0.066 | 112.811 | 0.000 |
| | Threshold | 0.010 | 2 | 0.005 | 8.422 | **0.000** |
| | Correction | 0.000 | 2 | 0.000 | 0.000 | 1.000 |
| | Threshold × Correction | 0.000 | 4 | 0.000 | 0.000 | 1.000 |
| | Error | 0.063 | 108 | 0.001 | | |
| | Total | 0.656 | 117 | | | |
| $A_{MI}/A_T$ | Model | 0.362 | 9 | 0.040 | 319.637 | 0.000 |
| | Threshold | 0.003 | 2 | 0.002 | 13.247 | **0.000** |
| | Correction | 0.000 | 2 | 0.000 | 0.005 | 0.995 |
| | Threshold × Correction | 0.000 | 4 | 0.000 | 0.001 | 1.000 |
| | Error | 0.014 | 108 | 0.000 | | |
| | Total | 0.376 | 117 | | | |
| $A_{MO}/A_T$ | Model | 0.194 | 9 | 0.022 | 27.845 | 0.000 |
| | Threshold | 0.007 | 2 | 0.003 | 4.438 | **0.014** |
| | Correction | 0.000 | 2 | 0.000 | 0.000 | 1.000 |
| | Threshold × Correction | 0.000 | 4 | 0.000 | 0.000 | 1.000 |
| | Error | 0.084 | 108 | 0.001 | | |
| | Total | 0.278 | 117 | | | |
| $A_{MI}/A_{ET}$ | Model | 0.492 | 9 | 0.055 | 429.770 | 0.000 |
| | Threshold | 0.000 | 2 | 0.000 | 0.744 | 0.478 |
| | Correction | 0.000 | 2 | 0.000 | 0.003 | 0.997 |
| | Threshold × Correction | 0.000 | 4 | 0.000 | 0.002 | 1.000 |
| | Error | 0.014 | 108 | 0.000 | | |
| | Total | 0.506 | 117 | | | |
| $A_{MO}/A_{ET}$ | Model | 0.206 | 9 | 0.023 | 122.201 | 0.000 |
| | Threshold | 0.001 | 2 | 0.000 | 1.465 | 0.236 |
| | Correction | 0.000 | 2 | 0.000 | 0.000 | 1.000 |
| | Threshold × Correction | 0.000 | 4 | 0.000 | 0.000 | 1.000 |
| | Error | 0.020 | 108 | 0.000 | | |
| | Total | 0.226 | 117 | | | |
| $A_{UI}/A_{ET}$ | Model | 0.605 | 9 | 0.067 | 57.288 | 0.000 |
| | Threshold | 0.027 | 2 | 0.013 | 11.358 | **0.000** |
| | Correction | 0.000 | 2 | 0.000 | 0.001 | 0.999 |
| | Threshold × Correction | 0.000 | 4 | 0.000 | 0.000 | 1.000 |
| | Error | 0.127 | 108 | 0.001 | | |
| | Total | 0.732 | 117 | | | |

Metrics used in accuracy variables are total area of mapped fire event ($A_{ET}$), total area of ground-truthing fire ($A_T$), area mapped inside ground-truthing perimeters ($A_{MI}$), area mapped outside ground-truthing perimeters ($A_{MO}$), and area undetected inside ground-ruthing perimeters ($A_{UI}$). All tests were conducted with n = 240 and a = 0.05.